

Study of the dependence of direct soft photon production on the jet characteristics in hadronic Z^0 decays

The DELPHI Collaboration

J. Abdallah²⁷, P. Abreu²⁴, W. Adam⁵⁷, P. Adzic¹³, T. Albrecht¹⁹, R. Alemany-Fernandez¹⁰, T. Allmendinger¹⁹, P.P. Allport²⁵, U. Amaldi³¹, N. Amapane⁴⁹, S. Amato⁵³, E. Anashkin³⁸, A. Andreatza³⁰, S. Andringa²⁴, N. Anjos²⁴, P. Antilogus²⁷, W.-D. Apel¹⁹, Y. Arnaud¹⁶, S. Ask¹⁰, B. Asman⁴⁸, J.E. Augustin²⁷, A. Augustinus¹⁰, P. Baillon¹⁰, A. Ballestrero⁵⁰, P. Bambade²², R. Barbier²⁹, D. Bardin¹⁸, G.J. Barker⁵⁹, A. Baroncelli⁴¹, M. Battaglia¹⁰, M. Baubillier²⁷, K.-H. Becks⁶⁰, M. Begalli⁸, A. Behrmann⁶⁰, E. Ben-Haim²⁷, N. Benekos³⁴, A. Benvenuti⁶, C. Berat¹⁶, M. Berggren²⁷, D. Bertrand³, M. Besancon⁴², N. Besson⁴², D. Bloch¹¹, M. Blom³³, M. Bluj⁵⁸, M. Bonesini³¹, M. Boonekamp⁴², P.S.L. Booth^{25,b}, G. Borisov²³, O. Botner⁵⁴, B. Bouquet²², T.J.V. Bowcock²⁵, I. Boyko¹⁸, M. Bracko⁴⁵, R. Brenner⁵⁴, E. Brodet³⁷, P. Bruckman²⁰, J.M. Brunet⁹, B. Buschbeck⁵⁷, P. Buschmann⁶⁰, M. Calvi³¹, T. Camporesi¹⁰, V. Canale⁴⁰, F. Carena¹⁰, N. Castro²⁴, F. Cavallo⁶, M. Chapkin⁴⁴, Ph. Charpentier¹⁰, P. Checchia³⁸, R. Chierici¹⁰, P. Chliapnikov⁴⁴, J. Chudoba¹⁰, S.U. Chung¹⁰, K. Cieslik²⁰, P. Collins¹⁰, R. Contri¹⁵, G. Cosme²², F. Cossutti⁵¹, M.J. Costa⁵⁵, D. Crennell³⁹, J. Cuevas³⁶, J. D'Hondt³, T. da Silva⁵³, W. Da Silva²⁷, G. Della Ricca⁵¹, A. De Angelis⁵², W. De Boer¹⁹, C. De Clercq³, B. De Lotto⁵², N. De Maria⁴⁹, A. De Min³⁸, L. de Paula⁵³, L. Di Ciaccio⁴⁰, A. Di Simone⁴¹, K. Doroba⁵⁸, J. Drees^{60,10}, G. Eigen⁵, T. Ekelof⁵⁴, M. Ellert⁵⁴, M. Elsing¹⁰, M.C. Espirito Santo²⁴, G. Fanourakis¹³, D. Fassouliotis^{13,4}, M. Feindt¹⁹, J. Fernandez⁴³, A. Ferrer⁵⁵, F. Ferro¹⁵, U. Flagmeyer⁶⁰, H. Foeth¹⁰, E. Fokitis³⁴, F. Fulda-Quenzer²², J. Fuster⁵⁵, M. Gandelman⁵³, C. Garcia⁵⁵, Ph. Gavillet¹⁰, E. Gaziz³⁴, R. Gokiel^{10,58}, B. Golob^{45,47}, G. Gomez-Ceballos⁴³, P. Goncalves²⁴, E. Graziani⁴¹, G. Grosdidier²², K. Grzelak⁵⁸, J. Guy³⁹, C. Haag¹⁹, A. Hallgren⁵⁴, K. Hamacher⁶⁰, K. Hamilton³⁷, S. Haug³⁵, F. Hauler¹⁹, V. Hedberg²⁸, M. Hennecke¹⁹, J. Hoffman⁵⁸, S.-O. Holmgren⁴⁸, P.J. Holt¹⁰, M.A. Houlden²⁵, J.N. Jackson²⁵, G. Jarlskog²⁸, P. Jarry⁴², D. Jeans³⁷, E.K. Johansson⁴⁸, P. Jonsson²⁹, C. Joram¹⁰, L. Jungermann¹⁹, F. Kapusta²⁷, S. Katsanevas²⁹, E. Katsoufis³⁴, G. Kernel⁴⁵, B.P. Kersevan^{45,47}, U. Kerzel¹⁹, B.T. King²⁵, N.J. Kjaer¹⁰, P. Kluit³³, P. Kokkinias¹³, C. Kourkoumelis⁴, O. Kouznetsov¹⁸, Z. Krumstein¹⁸, M. Kucharczyk²⁰, J. Lamsa¹, G. Leder⁵⁷, F. Ledroit¹⁶, L. Leinonen⁴⁸, R. Leitner³², J. Lemonne³, V. Lepeltier^{22,b}, T. Lesiak²⁰, W. Liebig⁶⁰, D. Liko⁵⁷, A. Lipniacka⁴⁸, J.H. Lopes⁵³, J.M. Lopez³⁶, D. Loukas¹³, P. Lutz⁴², L. Lyons³⁷, J. MacNaughton⁵⁷, A. Malek⁶⁰, S. Maltezos³⁴, F. Mandl⁵⁷, J. Marco⁴³, R. Marco⁴³, B. Marechal⁵³, M. Margoni³⁸, J.-C. Marin¹⁰, C. Mariotti¹⁰, A. Markou¹³, C. Martinez-Rivero⁴³, J. Masik¹⁴, N. Mastroiannopoulos¹³, F. Matorras⁴³, C. Matteuzzi³¹, F. Mazzucato³⁸, M. Mazzucato³⁸, R. Mc Nulty²⁵, C. Meroni³⁰, E. Migliore⁴⁹, W. Mitaroff⁵⁷, U. Mjoernmark²⁸, T. Moa⁴⁸, M. Moch¹⁹, K. Moenig^{10,12}, R. Monge¹⁵, J. Montenegro³³, D. Moraes⁵³, S. Moreno²⁴, P. Morettini¹⁵, U. Mueller⁶⁰, K. Muenich⁶⁰, M. Mulders³³, L. Mundim⁸, W. Murray³⁹, B. Muryn²¹, G. Myatt³⁷, T. Myklebust³⁵, M. Nassiakou¹³, F. Navarra⁶, K. Nawrocki⁵⁸, S. Nemecek¹⁴, R. Nicolaidou⁴², M. Nikolenko^{18,11}, A. Oblakowska-Mucha²¹, V. Obraztsov⁴⁴, A. Olshevski¹⁸, A. Onofre²⁴, R. Orava¹⁷, K. Osterberg¹⁷, A. Ouraou⁴², A. Oyanguren⁵⁵, M. Paganoni³¹, S. Paiano⁶, J.P. Palacios²⁵, H. Palka²⁰, Th.D. Papadopoulou³⁴, L. Pape¹⁰, C. Parkes²⁶, F. Parodi¹⁵, U. Parzefall¹⁰, A. Passeri⁴¹, O. Passon⁶⁰, L. Peralta²⁴, V. Perepelitsa^{55,56}, A. Perrotta⁶, A. Petrolini¹⁵, J. Piedra⁴³, L. Pieri⁴¹, F. Pierre⁴², M. Pimenta²⁴, E. Piotto¹⁰, T. Podobnik^{45,47}, V. Poireau¹⁰, M.E. Pol⁷, G. Polok²⁰, V. Pozdniakov¹⁸, N. Pukhaeva¹⁸, A. Pullia³¹, D. Radojicic³⁷, P. Rebecchi¹⁰, J. Rehn¹⁹, D. Reid³³, R. Reinhardt⁶⁰, P. Renton³⁷, F. Richard²², J. Ridky¹⁴, M. Rivero⁴³, D. Rodriguez⁴³, A. Romero⁴⁹, P. Ronchese³⁸, P. Roudeau²², T. Rovelli⁶, V. Ruhlmann-Kleider⁴², D. Ryabtchikov⁴⁴, A. Sadovsky¹⁸, L. Salmi¹⁷, J. Salt⁵⁵, C. Sander¹⁹, A. Savoy-Navarro²⁷, U. Schwickerath¹⁰, R. Sekulin³⁹, M. Siebel⁶⁰, A. Sisakian¹⁸, G. Smadja²⁹, O. Smirnova²⁸, A. Sokolov⁴⁴, A. Sopczak²³, R. Sosnowski⁵⁸, T. Spassov¹⁰, M. Stanitzki¹⁹, A. Stocchi²², J. Strauss⁵⁷, B. Stugu⁵, M. Szczekowski⁵⁸, M. Szeptycka⁵⁸, T. Szumlak²¹, T. Tabarelli³¹, F. Tegenfeldt⁵⁴, J. Timmermans^{33,a}, L. Tkatchev¹⁸, M. Tobin²⁵, S. Todorovova¹⁴, B. Tome²⁴, A. Tonazzo³¹, P. Tortosa⁵⁵, P. Travnicek¹⁴, D. Treille¹⁰, G. Tristram⁹, M. Trochimczuk⁵⁸, C. Troncon³⁰, M.-L. Turluer⁴², I.A. Tyapkin¹⁸, P. Tyapkin¹⁸, S. Tzamarias¹³, V. Uvarov⁴⁴, G. Valenti⁶, P. Van Dam³³, J. Van Eldik¹⁰, N. van Remortel², I. Van Vulpen¹⁰, G. Vegni³⁰, F. Veloso²⁴, W. Venus³⁹, P. Verdier²⁹, V. Verzi⁴⁰, D. Vilanova⁴², L. Vitale⁵¹, V. Vrba¹⁴, H. Wahlen⁶⁰, A.J. Washbrook²⁵

C. Weiser¹⁹, D. Wicke¹⁰, J. Wickens³, G. Wilkinson³⁷, M. Winter¹¹, M. Witek²⁰, O. Yushchenko⁴⁴, A. Zalewska²⁰, P. Zalewski⁵⁸, D. Zavrtnik⁴⁶, V. Zhuravlov¹⁸, N.I. Zimin¹⁸, A. Zintchenko¹⁸, M. Zupan¹³

¹Department of Physics and Astronomy, Iowa State University, Ames, IA 50011-3160, USA

²Physics Department, Universiteit Antwerpen, Universiteitsplein 1, 2610 Antwerpen, Belgium

³IIHE, ULB-VUB, Pleinlaan 2, 1050 Brussels, Belgium

⁴Physics Laboratory, University of Athens, Solonos Str. 104, 10680 Athens, Greece

⁵Department of Physics, University of Bergen, Allégaten 55, 5007 Bergen, Norway

⁶Dipartimento di Fisica, Università di Bologna and INFN, Viale C. Berti Pichat 6/2, 40127 Bologna, Italy

⁷Centro Brasileiro de Pesquisas Físicas, rua Xavier Sigaud 150, 22290 Rio de Janeiro, Brazil

⁸Inst. de Física, Univ. Estadual do Rio de Janeiro, rua São Francisco Xavier 524, Rio de Janeiro, Brazil

⁹Collège de France, Lab. de Physique Corpusculaire, IN2P3-CNRS, 75231 Paris Cedex 05, France

¹⁰CERN, 1211 Geneva 23, Switzerland

¹¹Institut Pluridisciplinaire Hubert Curien, Université de Strasbourg, 67037 Strasbourg Cedex 2, France

¹²*Present address:* DESY-Zeuthen, Platanenallee 6, 15735 Zeuthen, Germany

¹³Institute of Nuclear Physics, N.C.S.R. Demokritos, P.O. Box 60228, 15310 Athens, Greece

¹⁴FZU, Inst. of Phys. of the C.A.S. High Energy Physics Division, Na Slovance 2, 182 21 Praha 8, Czech Republic

¹⁵Dipartimento di Fisica, Università di Genova and INFN, Via Dodecaneso 33, 16146 Genova, Italy

¹⁶Institut des Sciences Nucléaires, IN2P3-CNRS, Université de Grenoble 1, 38026 Grenoble Cedex, France

¹⁷Helsinki Institute of Physics and Department of Physical Sciences, University of Helsinki, P.O. Box 64, 00014 Helsinki, Finland

¹⁸Joint Institute for Nuclear Research, Dubna, Head Post Office, P.O. Box 79, 101 000 Moscow, Russian Federation

¹⁹Institut für Experimentelle Kernphysik, Universität Karlsruhe, Postfach 6980, 76128 Karlsruhe, Germany

²⁰Institute of Nuclear Physics PAN, Ul. Radzikowskiego 152, 31142 Krakow, Poland

²¹Faculty of Physics and Nuclear Techniques, University of Mining and Metallurgy, 30055 Krakow, Poland

²²LAL, Univ Paris-Sud, CNRS/IN2P3, Orsay, France

²³School of Physics and Chemistry, University of Lancaster, Lancaster LA1 4YB, UK

²⁴LIP, IST, FCUL - Av. Elias Garcia, 14-1º, 1000 Lisboa Codex, Portugal

²⁵Department of Physics, University of Liverpool, P.O. Box 147, Liverpool L69 3BX, UK

²⁶Dept. of Physics and Astronomy, Kelvin Building, University of Glasgow, Glasgow G12 8QQ, UK

²⁷LPNHE, IN2P3-CNRS, Univ. Paris VI et VII, Tour 33 (RdC), 4 place Jussieu, 75252 Paris Cedex 05, France

²⁸Department of Physics, University of Lund, Sölvegatan 14, 223 63 Lund, Sweden

²⁹IPNL, IN2P3-CNRS, Université Claude Bernard de Lyon, 69622 Villeurbanne Cedex, France

³⁰Dipartimento di Fisica, Università di Milano and INFN-MILANO, Via Celoria 16, 20133 Milan, Italy

³¹Dipartimento di Fisica, Univ. di Milano-Bicocca and INFN-MILANO, Piazza della Scienza 3, 20126 Milan, Italy

³²IPNP of MFF, Charles Univ., Areal MFF, V Holesovickach 2, 180 00 Praha 8, Czech Republic

³³NIKHEF, Postbus 41882, 1009 DB Amsterdam, The Netherlands

³⁴Physics Department, National Technical University, Zografou Campus, 15773 Athens, Greece

³⁵Physics Department, University of Oslo, Blindern, 0316 Oslo, Norway

³⁶Dpto. Fisica, Univ. Oviedo, Avda. Calvo Sotelo s/n, 33007 Oviedo, Spain

³⁷Department of Physics, University of Oxford, Keble Road, Oxford OX1 3RH, UK

³⁸Dipartimento di Fisica, Università di Padova and INFN, Via Marzolo 8, 35131 Padua, Italy

³⁹Rutherford Appleton Laboratory, Chilton, Didcot OX11 0QX, UK

⁴⁰Dipartimento di Fisica, Università di Roma II and INFN, Tor Vergata, 00173 Rome, Italy

⁴¹Dipartimento di Fisica, Università di Roma III and INFN, Via della Vasca Navale 84, 00146 Rome, Italy

⁴²DAPNIA/Service de Physique des Particules, CEA-Saclay, 91191 Gif-sur-Yvette Cedex, France

⁴³Instituto de Física de Cantabria (CSIC-UC), Avda. los Castros s/n, 39006 Santander, Spain

⁴⁴Inst. for High Energy Physics, Serpukov P.O. Box 35, Protvino (Moscow Region), Russian Federation

⁴⁵J. Stefan Institute, Jamova 39, 1000 Ljubljana, Slovenia

⁴⁶Laboratory for Astroparticle Physics, University of Nova Gorica, Kostanjevska 16a, 5000 Nova Gorica, Slovenia

⁴⁷Department of Physics, University of Ljubljana, 1000 Ljubljana, Slovenia

⁴⁸Fysikum, Stockholm University, Box 6730, 113 85 Stockholm, Sweden

⁴⁹Dipartimento di Fisica Sperimentale, Università di Torino and INFN, Via P. Giuria 1, 10125 Turin, Italy

⁵⁰INFN, Sezione di Torino and Dipartimento di Fisica Teorica, Università di Torino, Via Giuria 1, 10125 Turin, Italy

⁵¹Dipartimento di Fisica, Università di Trieste and INFN, Via A. Valerio 2, 34127 Trieste, Italy

⁵²Istituto di Fisica, Università di Udine and INFN, 33100 Udine, Italy

⁵³Univ. Federal do Rio de Janeiro, C.P. 68528 Cidade Univ., Ilha do Fundão, 21945-970 Rio de Janeiro, Brazil

⁵⁴Department of Radiation Sciences, University of Uppsala, P.O. Box 535, 751 21 Uppsala, Sweden

⁵⁵IFIC, Valencia-CSIC, and D.F.A.M.N., U. de Valencia, Avda. Dr. Moliner 50, 46100 Burjassot (Valencia), Spain

⁵⁶On leave of absence from: ITEP, 117259 Moscow, Russian Federation

⁵⁷Institut für Hochenergiephysik, Österr. Akad. d. Wissensch., Nikolsdorfergasse 18, 1050 Vienna, Austria

⁵⁸Inst. Nuclear Studies and University of Warsaw, Ul. Hoza 69, 00681 Warsaw, Poland

⁵⁹*Present address:* University of Warwick, Coventry CV4 7AL, UK

⁶⁰Fachbereich Physik, University of Wuppertal, Postfach 100 127, 42097 Wuppertal, Germany

Received: 1 July 2009 / Revised: 17 March 2010 / Published online: 22 April 2010

© The Author(s) 2010. This article is published with open access at Springerlink.com

Abstract An analysis of the direct soft photon production rate as a function of the parent jet characteristics is presented, based on hadronic events collected by the DELPHI experiment at LEP1. The dependences of the photon rates on the jet kinematic characteristics (momentum, mass, etc.) and on the jet charged, neutral and total hadron multiplicities are reported. Up to a scale factor of about four, which characterizes the overall value of the soft photon excess, a similarity of the observed soft photon behavior to that of the inner hadronic bremsstrahlung predictions is found for the momentum, mass, and jet charged multiplicity dependences. However for the dependence of the soft photon rate on the jet neutral and total hadron multiplicities a prominent difference is found for the observed soft photon signal as compared to the expected bremsstrahlung from final state hadrons. The observed linear increase of the soft photon production rate with the jet total hadron multiplicity and its strong dependence on the jet neutral multiplicity suggest that the rate is proportional to the number of quark pairs produced in the fragmentation process, with the neutral pairs being more effectively radiating than the charged ones.

1 Introduction

Recent analysis of the soft photon production in hadronic decays of the Z^0 studied with the DELPHI detector at LEP1 [1] revealed a significant excess of soft photons deep inside jets as compared to the predictions of parton shower models [2–6] for the photon rates induced by hadrons decaying radiatively (most of the photons coming from π^0 's). The photon kinematic range was defined in [1] as: $0.2 < E_\gamma < 1$ GeV, $p_T < 80$ MeV/c, the p_T being the photon transverse momentum with respect to the parent jet direction. Furthermore, the observed signal was much greater than the level of the inner hadronic bremsstrahlung, which according to the QED predictions (see [7, 8]) was expected to be the dominant source of the direct soft photons in this kinematic region. Expressed in terms of the predicted bremsstrahlung rate, the observed signal was found to be $3.4 \pm 0.2 \pm 0.8$ for the data uncorrected for the detection efficiency, and $4.0 \pm 0.3 \pm 1.0$ for the corrected data (the first errors are statistical, the second ones are systematic).

The observation of the excess of soft photons in hadronic events of Z^0 decays reported in [1] is indeed a further contribution to the collection of the anomalous soft photon effects found earlier in reactions of multiple hadron production in

several hadronic beam experiments at high energy [9–14], all at the photon c.m.s. rapidities $y > 1.2$.¹ Known for more than 20 years, they however still lack a theoretical explanation, in spite of being under active investigation. Reviews of the theoretical approaches to the problem can be found in [17, 18] (see also Refs. [13–33] in [1]).

On the other hand, no deviation of the photon production rates and/or other radiation characteristics has been observed compared to the predictions based on QED for effects of pure electroweak nature. For example, the electron inner bremsstrahlung in e^+e^- collisions at LEP (initial state radiation, ISR) was an important experimental effect, with which all the LEP experiments had to contend. No deviation of the ISR characteristics from those expected from theory was observed, either at the Z^0 or at high energy (see e.g. the DELPHI studies [19–21]). A direct study of the muon inner bremsstrahlung in $\mu^+\mu^-$ decays of the Z^0 (final state radiation, FSR) in events collected by the DELPHI experiment at LEP1, with the same experimental method as employed in [1], has shown a good agreement of the observed photon production characteristics with those expected from the bremsstrahlung predictions [22].

Thus, the soft photon anomaly seems to be restricted to the processes of multiple hadron production, i.e. it is rooted in strong interaction physics. Nevertheless it is clear that the development of a theory resolving this long-standing problem currently requires further experimental information. The process of e^+e^- annihilation to hadrons, in which events with well defined jet structure are produced, presents a suitable opportunity to meet the challenge. Therefore this paper continues the investigation of events from reaction

$$e^+e^- \rightarrow Z^0 \rightarrow \text{direct soft } \gamma + \text{hadrons} \quad (1)$$

begun in paper [1]. The aim of the present analysis is the study of several dependences of the direct soft photon production on the parent jet characteristics, to which various models treating the anomalous radiation may be sensitive. Among these characteristics are the jet momentum, mass, net charge and the jet particle multiplicities. The last dependence is presented subdivided into three branches: dependences on charged, neutral and total (neutral + charged) multiplicities of the jet. The kinematic region of this analysis is kept the same as in [1]. Based on the results of this study, indications for a possible localization of the source of anomalous soft photons are obtained: such a source may be the creation out of the QCD vacuum of the lightest (u, d)

^a e-mail: jan.timmermans@cern.ch

^b Deceased.

¹For the sake of completeness we mention two studies of soft photons at central and slightly backward c.m.s. rapidities [15, 16] in which no photon excess over the expected bremsstrahlung level was observed.

quarks, with their further evolution during the processes of the parton shower development and hadronization.

This paper is organized as follows. Section 2 deals with the calculation of the inner hadronic bremsstrahlung. Section 3 provides a description of the apparatus, software, and the experimental method applied. Section 4 describes the selection cuts and data samples. In Sect. 5 the definition of variables used in the analysis is given. Systematic uncertainties arising from various elements of the analysis method, and their estimates are presented in Sect. 6. In Sect. 7 the main results of the analysis are given. Discussion of the obtained results and their possible interpretation, with emphasis on the strong signal dependence on the jet neutral multiplicity, are given in Sect. 8. Finally, Sect. 9 provides a summary and conclusions.

2 Bremsstrahlung calculations

The production rate for both ISR and inner bremsstrahlung from final hadronic states in the soft photon region can be calculated simultaneously using a universal formula derived from Low [7] with a modification suggested by Haissinski [23–25]:

$$\frac{dN_\gamma}{d^3\vec{k}} = \frac{\alpha}{(2\pi)^2} \frac{1}{E_\gamma} \int d^3\vec{p}_1 \dots d^3\vec{p}_N \times \sum_{i,j} \eta_i \eta_j \frac{(\vec{p}_{i\perp} \cdot \vec{p}_{j\perp})}{(P_i K)(P_j K)} \frac{dN_{\text{hadrons}}}{d^3\vec{p}_1 \dots d^3\vec{p}_N}. \quad (2)$$

Here K and \vec{k} denote photon four- and three-momenta, P are the four-momenta of beam e^+ , e^- and N charged outgoing hadrons, and $\vec{p}_1 \dots \vec{p}_N$ are the three-momenta of the hadrons; $\vec{p}_{i\perp} = \vec{p}_i - (\vec{n} \cdot \vec{p}_i) \cdot \vec{n}$ and \vec{n} is the photon unit vector, $\vec{n} = \vec{k}/k$; $\eta = 1$ for the beam electron and for positive outgoing hadrons, $\eta = -1$ for the beam positron and negative outgoing hadrons, and the sum is extended over all the $N + 2$ charged particles involved; the last factor in the integrand is a differential hadron production rate.

Note, formula (2) is completely equivalent, from a theoretical point of view, to the analogous one, applied for calculation of the inner hadronic bremsstrahlung in [9, 10, 17] and considered to be standard in textbooks on electrodynamics. It differs from the latter by the numerator $(\vec{p}_{i\perp} \cdot \vec{p}_{j\perp})$, used to replace the four-dimensional scalar product $-(P_i P_j)$. When dealing with relativistic particles, the advantage of such a replacement is essential and is based on the following. Both formulae operate, in general, by terms of big absolute values adjusted in such a way that they cancel each other in the sum almost completely due to η_i, η_j alternate signs. However this “fine tuning” which is rooted in the gauge invariance of electrodynamics and reflects the charge conservation law, is achieved in numerical calculations more eas-

ily with formula (2). Therefore, when using detected particle spectra in the bremsstrahlung calculations, formula (2) is more stable with respect to the particle loss and measurement errors as compared to the standard one. Moreover, even in the case of using precise Monte Carlo spectra for the calculations, as was done in [1, 11–14, 22], the implementation of formula (2) should be preferred in computing the bremsstrahlung as giving smaller fluctuations of the sum terms for the specific particle and photon momentum configurations leading to extremely low values of denominators in formula (2) (so called collinear singularity).

Formula (2), as well as its standard analog, describes both initial state radiation from the colliding e^+e^- , and the inner bremsstrahlung from the final hadronic states. However, it was demonstrated in [1] that the ISR is rather small in the range of the photon polar angles to the beam Θ_γ used in this analysis (barrel region), being about 1.5% of the total hadronic inner bremsstrahlung. The situation changes little even when there are very few charged particles inside the jet. For example, for charged jet multiplicities between 0 and 2 (which corresponds to the first bin of the photon rate distribution over the N_{ch} variable defined below, see Sect. 5.3) the ISR rate in the chosen kinematic range is at the level of about 4% of the inner hadronic bremsstrahlung yield in this bin. Therefore the ISR contribution is marginal in the predicted bremsstrahlung rates.

Similarly, the yield of final state radiation from quarks of Z^0 disintegrations, calculated within the standard perturbative approach implemented in the LUND fragmentation model [2–4, 26], is small too. It was shown in [1] where this approach was used to evaluate the bremsstrahlung radiation off quarks, that it is at the level of 3% of the inner hadronic bremsstrahlung within the kinematic range considered. The reasons for this suppression are the fractional quark charges (which give an attenuation factor of about 1/4) and large quark virtualities which are intrinsic for this approach.

The treatment of the three listed bremsstrahlung sources (inner hadronic bremsstrahlung, ISR and the radiation off quarks of Z^0 disintegrations) was different in the Monte Carlo (MC) stream as described below (Sect. 3.2).

3 Experimental technique

3.1 The DELPHI detector

The DELPHI detector is described in detail in [27, 28]. The following is a brief description of the subdetector units relevant for this analysis: the main tracker of the DELPHI detector, the Time Projection Chamber (TPC), the barrel electromagnetic calorimeter, the High density Projection Chamber (HPC), and the hadronic calorimeter (HCAL).

In the DELPHI reference frame the z axis is taken along the direction of the e^- beam. The angle Θ is the polar angle

defined with respect to the z -axis, Φ is the azimuthal angle around this axis and R is the distance from this axis.

The TPC covered the angular range from 20° to 160° in Θ and extended from 30 cm to 122 cm in R . It provided up to 16 space points for pattern recognition and ionization information extracted from 192 wires. The momentum threshold for charged particles entering the TPC was approximately $100 \text{ MeV}/c$.

The HPC was used for the detection of high energy photons, which originate in hadronic events mainly from the decays of neutral pions. The HPC lay immediately outside the tracking detectors and covered the angles Θ from 43° to 137° . It had eighteen radiation lengths for perpendicular incidence, and its energy resolution was $\Delta E/E = 0.31/E^{0.44} \oplus 0.027$ where E is in units of GeV [29]. It had a high granularity and provided a sampling of shower energies from nine layers in depth. The angular precisions for high energy photons were $\pm 1.0 \text{ mrad}$ in Θ and $\pm 1.7 \text{ mrad}$ in Φ .

The HCAL was installed in the return yoke of the DELPHI solenoid and provided a relative precision on the measured energy of $\Delta E/E = 1.12/\sqrt{E} \oplus 0.21$. It was used for the detection of K_L^0 's and neutrons.

3.2 Monte Carlo generators

The principal Monte Carlo data sets used in this analysis were produced with the JETSET 7.3 PS generator [2–4], based on the LUND string model [30], with parameters adjusted according to previous QCD studies [31–33]. For the test of possible systematic biases, another standard generator, ARIADNE 4.6 [5] with parameters adjusted by the DELPHI tuning [33] was also used.²

No generation of bremsstrahlung photons from the final state hadrons was implemented in these MC generators. On the other hand, initial state radiation and photon radiation from quarks of Z^0 disintegrations calculated with the photon implementation in JETSET [26] were involved in all the generations.

The generated events were fed into the DELPHI detector simulation program DELSIM [28] in order to produce data which are as close as possible to the real raw data. These data were then treated by the reconstruction and analysis programs in exactly the same way as the real data.

In order to evaluate the contamination from the $Z^0 \rightarrow \tau^+ \tau^-$ channel MC events produced with the KORALZ 4.0

generator [34] and passed through a full detector simulation and the analysis procedure were used.

Finally, the generator DYMU3 [35, 36] was used to check the applicability of formula (2) in our kinematic region, see Sect. 6.3.

3.3 Detection of soft photons

The experimental technique employed for the detection of soft photons in this analysis was the same as in [1], based on the reconstruction of the photons converted in front of the TPC. The following is a brief description of the method implemented for the photon reconstruction and main characteristics of the detected photons obtained with it.

The photon conversions were reconstructed by an algorithm that examined tracks reconstructed in the TPC. A search was made along each TPC track for the point where the tangent of its trajectory points directly to the beam spot in the $R\Phi$ projection. Under the assumption that the opening angle of the electron-positron pair is zero, this point represented a possible photon conversion position at radius R . All tracks which had a solution R that was more than one standard deviation away from the primary vertex, as defined by the beam spot, were considered to be conversion candidates. If two oppositely charged conversion candidates were found with compatible conversion point parameters they were linked together to form the converted photon. The following selection criteria were imposed:

- the Φ difference between the two conversion points was at most 30 mrad ;
- the difference between the polar angles Θ of the two tracks was at most 15 mrad ;
- at least one of the tracks should have no associated hits in front of the reconstructed mean conversion radius.

For the pairs fulfilling these criteria a χ^2 was calculated from $\Delta\Theta$, $\Delta\Phi$ and the difference of the reconstructed conversion radii ΔR in order to find the best combinations in cases where there were ambiguous associations. A constrained fit was then applied to the electron-positron pair candidate which forced a common conversion point with zero opening angle and collinearity between the momentum sum and the line from the beam spot to the conversion point.

The quality of the photon reconstruction in both, the real data (RD) and MC events, the latter being produced as described in Sect. 3.2, was high, as can be judged comparing π^0 peaks in the RD and MC $\gamma - \gamma$ mass distributions obtained with converted photons and shown in Fig. 8 of [1]. The almost precise identity of these peaks, together with their widths of less than $5 \text{ MeV}/c^2$, demonstrate that the detection and analysis procedures of the converted photons in the DELPHI detector are well understood; this statement is supported also by the results of the DELPHI papers [29, 37],

²As noticed in [1], ARIADNE tends to underestimate the production of photons in the range of the photon $p_T < 80 \text{ MeV}/c$. A special test, which exploited the $SU(2)$ symmetry of the strong interactions, using artificial photons produced from charged pions (similar to that described in Sect. 6.5 of [1]), has shown better performance of JETSET versus variables under study, as compared to ARIADNE. This explains why JETSET was chosen as the principal generator in this analysis.

in which the converted photons were involved in the analysis.

Selection of photons for this analysis was done under the following cuts:

- $20^\circ \leq \Theta_\gamma \leq 160^\circ$;
- $5 \text{ cm} \leq R_{\text{conv}} \leq 50 \text{ cm}$, where R_{conv} is the conversion radius;
- $200 \text{ MeV} \leq E_\gamma \leq 1 \text{ GeV}$.

The photon detection efficiency, i.e. conversion probability combined with the reconstruction efficiency, was determined with the MC events and parameterized against two variables. The first variable, E_γ , was used to describe a fast variation of the efficiency within the energy range under study, from almost zero at 0.2 GeV up to 5–6% at 1 GeV (a typical behavior of the efficiency with E_γ can be seen in Fig. 1 of paper [1]). For interpolation of the efficiency, it was fitted by a 2nd order polynomial or by the form $a - b \times \exp[-c(E_\gamma - 0.2)]$ with a $\chi^2/\text{n.d.f.}$ close to 1 in both cases; the difference in the corrected photon rates obtained with the two interpolation curves was about 2%.

The second variable of the efficiency parameterization is related to the jet characteristic under investigation, i.e. the efficiencies were determined separately in every bin of the jet parameter under study. The weak dependences of the photon detection efficiency on several additional variables treated in [1] (the photon polar angle to the beam, Θ_γ , the photon polar angle to the parent jet axis, θ_γ , etc.) were decided to be averaged over in this analysis.

The validity of the efficiency finding can be considered as confirmed by the results of DELPHI paper [22] in which the inner bremsstrahlung off muons from Z^0 dimuon decays was studied by applying the efficiencies obtained as described above, and the photon signal was found to be in good agreement with the theoretical expectations. More generally, the muon inner bremsstrahlung study [22], being carried out with the same methods of photon detection and analysis as in the current study, gives them further credibility.

The accuracy of the converted photon energy measurement was about $\pm 1.6\%$ in the given kinematic range, as follows from the MC studies. This estimate was confirmed by extracting the photon energy resolution from the widths of π^0 peaks in the RD and MC $\gamma - \gamma$ mass distributions obtained with converted photons as shown in Fig. 8 of [1].

The angular precision of the photon direction reconstruction was determined with the MC data and was found to be of a Breit-Wigner shape, as expected for the superposition of many Gaussian distributions of varying width [38]. The full widths (Γ 's) of the $\Delta\Theta_\gamma$ and $\Delta\Phi_\gamma$ distributions were 4 and 5 mrad, respectively (for details see [1]).

4 Data selection

Events involving the hadronic decays of the Z^0 from the DELPHI data of the 1992 to 1995 running periods were used in this analysis.

Selection of the hadronic events was standard, based on large event charged multiplicity ($N_{\text{ch}}^{\text{evt}} \geq 5$) and high visible energy ($E_{\text{vis}} \geq 0.2E_{\text{cm}}$). In addition, the condition $|\cos \Theta_{\text{thrust}}| < 0.95$ was imposed, where Θ_{thrust} is the angle between the thrust axis and the beam direction. These criteria correspond to an efficiency of $(95.2 \pm 0.2)\%$, with a general $Z^0 \rightarrow \tau^+\tau^-$ contamination of $(0.5 \pm 0.1)\%$. The apparently low τ background is concentrated in small multiplicity events and may contaminate essentially the low jet multiplicity samples. Therefore a further suppression of the τ events has been achieved as described below.

First, the electron and muon anti-tagging was applied to the events of low multiplicity, defined as having $N_{\text{ch}}^{\text{evt}} \leq 7$. This method decreased the $\tau\tau$ background by 25%. Then two additional selections aimed at the $\tau\tau$ events suppression were implemented. The first one required that the jet masses in the low multiplicity events exceeded $2 \text{ GeV}/c^2$, with an exception for the jets having two or less charged particles: for such jets the lower mass cut was weakened, being at $1 \text{ GeV}/c^2$. The second $\tau\tau$ rejection method was based on the impact parameter analysis using the fact that the fraction of $\tau\tau$ events with $N_{\text{ch}}^{\text{evt}} \geq 5$ (i.e. surpassing the minimal $N_{\text{ch}}^{\text{evt}}$ multiplicity cut described above) is dominated by the τ hadronic decays containing at least one secondary interaction of the decay products which increases the originally low $\tau\tau$ event multiplicity. This leads to a considerably increased value of the sum of the track impact parameters in the $R\Phi$ projection in the $\tau\tau$ events as compared to hadronic events of the same multiplicity. Thus, only those small multiplicity events were selected in which the sum of the impact parameters in the $R\Phi$ projection over all charged particle tracks was below 1 cm (an analogous cut on the sum of the z projection impact parameters was found to be ineffective for further $\tau\tau$ background suppression). Together with the electron and muon anti-tagging these selections resulted in additional $\tau\tau$ background suppression by a factor of 5.9, while keeping the hadronic event efficiency at the level of $(94.7 \pm 0.2)\%$. The differential rates of photons from the $\tau\tau$ background (in the bins of the jet multiplicity variables defined in Sect. 5) will be given below, in the analysis section. It should be noted, that being deduced from $\tau\tau$ MC events they can be underestimated (by an unknown factor, not exceeding however 1.1–1.6 as follows from our special study of $\tau\tau$ events), if anomalous soft photons are produced in the hadronic tau decays also.

A total of 3 435 173 events of real data was selected under these cuts and compared to 12.1×10^6 MC events, produced as described in Sect. 3.2, selected under the same criteria as

the RD, and properly distributed over all the running periods.

Jets were reconstructed using the detected charged and neutral particles of the event, the charged particles being selected by applying the following criteria:

- $p > 200 \text{ MeV}/c$;
- $\Delta p/p < 100\%$;
- $20^\circ \leq \Theta \leq 160^\circ$;
- track length $> 30 \text{ cm}$;
- impact parameters below 4 and 10 cm in the $R\Phi$ and z projections, respectively.

The neutral particles were taken within the geometrical acceptances of the subdetectors in which they were reconstructed, within the selection criteria of the appropriate sub-detector pattern recognition codes [27, 28], without additional cuts. This effectively means that the detection threshold was about 400 MeV.

To reconstruct jets, the LUCCLUS code [39–41] with a fixed resolution parameter $d_{\text{join}} = 3 \text{ GeV}/c$ was used. Only jets containing no identified electrons (positrons) and satisfying the condition $30^\circ \leq \Theta_{\text{jet}} \leq 150^\circ$ were taken for the analysis. The minimum jet momentum was required to be 5 GeV/c.

Photons were selected using the cuts described in Sect. 3.3. A total of 694 530 converted photons was selected in the RD and 2 368 641 converted photons in the MC.

5 Specifying the analysis variables

5.1 Signal definition

As representatives of the photon rates the distributions of the p_T , the photon transverse momentum with respect to the jet direction, corrected for the detection efficiency were chosen (as mentioned above, only photons within the energy range of 0.2–1 GeV are considered). To quantify the excess, the difference of the rates between the RD and MC (the latter being normalized to the statistics of the RD events and corrected by the recalibration procedure, see [1] and Sect. 6.2.2 of this work) was integrated in the p_T interval from 0 to 80 MeV/c and the value obtained was defined as a signal.

5.2 Jet momentum

The jet momentum, p_{jet} , is defined as the vector sum of 3-momenta of all charged and neutral particles belonging to a given jet. The distributions of this variable obtained with both, the real and the MC data, are shown in Fig. 1a. Due to uncertainties in the determination of the jet constituent momenta and lost particles, this variable is not accurately measured (which can be seen also from Fig. 1a, with the distributions showing the maximum at 40 GeV/c, shifted from

the expected value of 45.6 GeV/c, and a tail extending up to 60 GeV/c). In order to evaluate the accuracy of the jet momentum reconstruction a comparison of the p_{jet} composed of the *measured* particle momenta with the vector sum of momenta of the *generated* particles (i.e. before transporting them through the detector), assigned to a given jet, was done using the MC data. The assignment procedure was the following.

First, only stable and quasi-stable particles (π^+ , π^- , K^+ , K^- , p , \bar{p} , and muons) were selected among the generated charged particles, the selection cut (200 MeV/c) being applied to them, similarly to the detected charged particles (see Sect. 4). Analogously, among the generated neutral particles only photons, K_L^0 's and neutrons were selected, imposing a cut at 400 MeV/c. Then for every selected *generated* particle a loop on jets (found by LUCCLUS with *detected* particles) was organized, calculating the generated particle opening angle to the jet axis. A generated particle has been assigned to that jet to which its opening angle was minimal. Note, this assignment procedure was also applied when defining, at the generator level, all the analysis variables described below.

The scatter plot of the reconstructed jet momenta, p_{jet} , versus jet momenta at the generator level determined via the procedure described above is shown in Fig. 2a. It is seen that the plot is dominated by the main diagonal (which corresponds to the equality of the generated and measured jet momenta) up to about 30 GeV/c where the accumulation of events near the diagonal starts to spread (note, the measured jet momenta exceeding $p_{\text{max}} = 0.5E_{\text{cm}}/c$ were reduced to that value in the plot, as well as in the analysis in general). The spread defined the bin size in the momentum variable employed in this work, chosen to be 5 GeV/c. To supply further information on the momentum bias, the mean values of the reconstructed and generated momentum distributions in the individual p_{jet} bins are given in Table 1 of the analysis section.

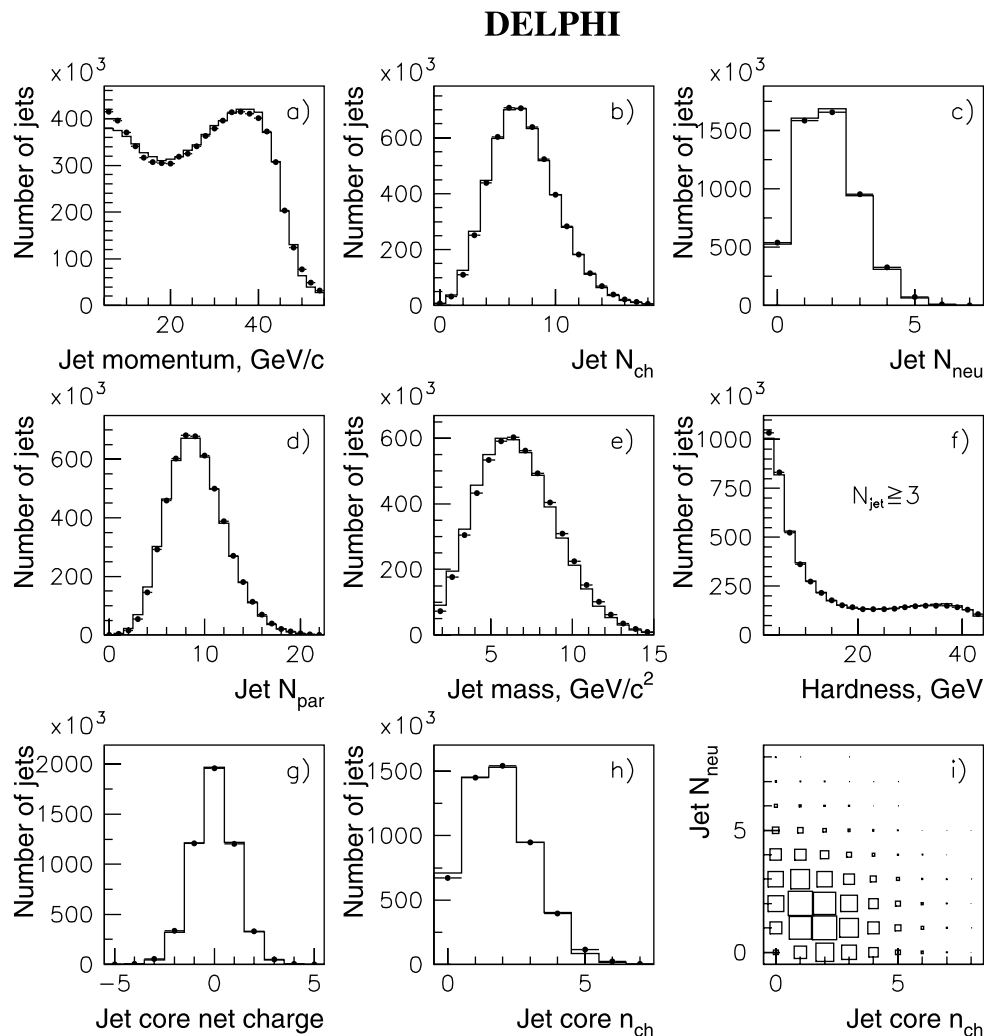
Closely related to the jet momentum, p_{jet} , is the jet energy E_{jet} , which can be defined as the sum of the energies of jet particles (assuming pion masses for them). This variable will not be used as an independent one, entering however into the definitions of other variables, the jet mass and hardness, see Sect. 5.6.

In what follows, all the jet variables (with one exception for the hardness κ_J) will be defined for jets having momenta $p_{\text{jet}} > 20 \text{ GeV}/c$ (for the motivation of this cut see Sect. 7.1).

5.3 Jet charged multiplicity

The jet charged multiplicity, N_{ch} , is defined as the number of charged particles measured in the DELPHI tracking system, as described in more detail in [28], with the tracks satisfying the selection criteria listed in Sect. 4 and pertaining to a given jet. The distributions of this variable for the RD

Fig. 1 (a) to (h), the distributions of the variables used in this analysis, obtained with both, the real data (*points*), and with the MC (*histograms*); (a) jet momentum; (b) jet charged multiplicity; (c) jet neutral multiplicity; (d) jet total multiplicity; (e) jet mass; (f) hardness variable, κ_J ; (g) jet core net charge; (h) jet core charged multiplicity. The panel (i) shows the correlation plot of the jet N_{neu} vs the jet core n_{ch}



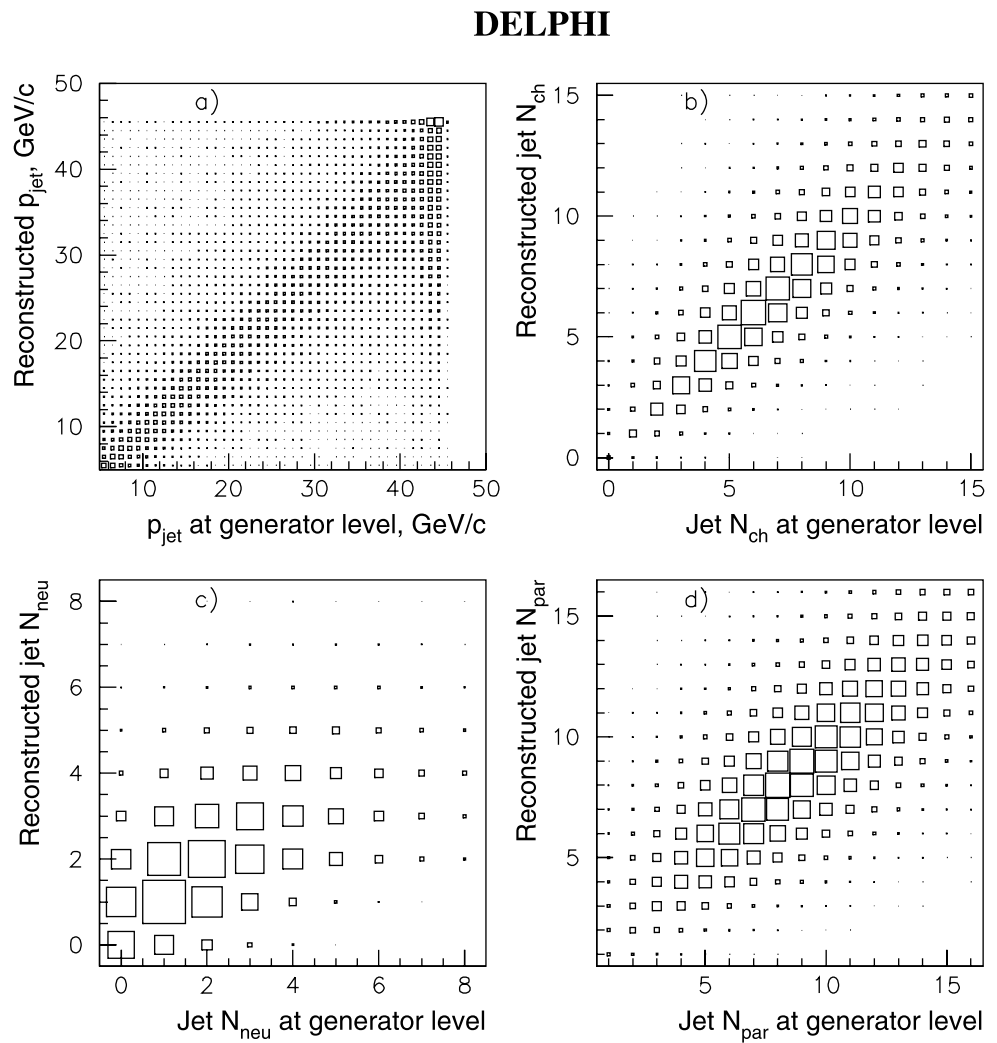
and MC are shown in Fig. 1b. At the generator level, the jet charged multiplicity, $N_{\text{ch}}^{\text{gen}}$, is defined as the number of stable charged particles produced in the primary fragmentation or in the decays of particles with lifetimes shorter than 3×10^{-10} s which belong to a given jet. In particular, the charged particles from K_s^0 and Λ decays were included in the $N_{\text{ch}}^{\text{gen}}$, irrespectively of how far from the interaction point the decay occurred, while the charged particles from K_L^0 decay were not.

As in the previous case, with the jet momenta, one faces the problem of associating an observed charged multiplicity of a jet N_{ch} to the “true” one. Usually this problem is solved by making use of the multiplicity corrections with a matrix $P(j, i)$, whose elements, defined with the MC data, are the probabilities of a jet with observed charged multiplicity j to have a “true” charged multiplicity i (the latter being determined via an assignment procedure analogous to that described in the previous section, this time for the generated charged particles only). Then the observed multiplicity is corrected accordingly to these probabilities. This

method reproduces perfectly the distributions of the jet multiplicities, but being purely probabilistic it is not applicable when the jet multiplicity has to be used as an argument on a jet-by-jet basis. This requires a special consideration of the problem.

The effect of the multiplicity migration is illustrated by Fig. 2b where the scatter plot of the reconstructed jet N_{ch} multiplicity versus the jet charged multiplicity at the generator level is displayed. It shows the following features: the cells on the main diagonal are the most populated; non-diagonal elements are almost symmetric with respect to the diagonal, though some small prevalence of the under-diagonal terms relative to the above-diagonal ones can be seen, which corresponds to track losses. In order to keep the N_{ch} systematic bias transparent, columns with the generated charged multiplicity mean values and their r.m.s. are given in Table 2 to be compared with the N_{ch} . It can be seen that the bias of the N_{ch} variable is always comparable to (generally, smaller than) the N_{ch} half bin widths employed, and therefore it was considered to be admissible in the cur-

Fig. 2 (a) Reconstructed jet momentum p_{jet} vs jet momentum at the generator level; (b) reconstructed jet N_{ch} multiplicity vs jet charged multiplicity at the generator level; (c) reconstructed jet N_{neu} multiplicity vs jet neutral multiplicity at the generator level; (d) reconstructed jet N_{par} multiplicity vs jet particle multiplicity at the generator level



rent study. The validity of this assumption was tested when the main results of a given analysis were obtained and used to model the effect of the photon rate bias due to multiplicity migration, with the effect being found to be negligible.

5.4 Jet neutral particle multiplicity

The term “neutral particle” specifies a neutral hadron satisfying the selection criteria described below. The criteria are aimed at counting neutral hadrons (which are π^0 's mainly) using the DELPHI electromagnetic calorimeter (HPC) and converted photons. Also the DELPHI hadron calorimeter (HCAL) was used to detect a small fraction of K_L^0 's and neutrons (antineutrons). The detected neutral showers (the showers which cannot be associated to any charged particle track) and converted photons were treated in the following way:

- HPC showers with the energy within the range from 1 to 6 GeV were considered as photons;

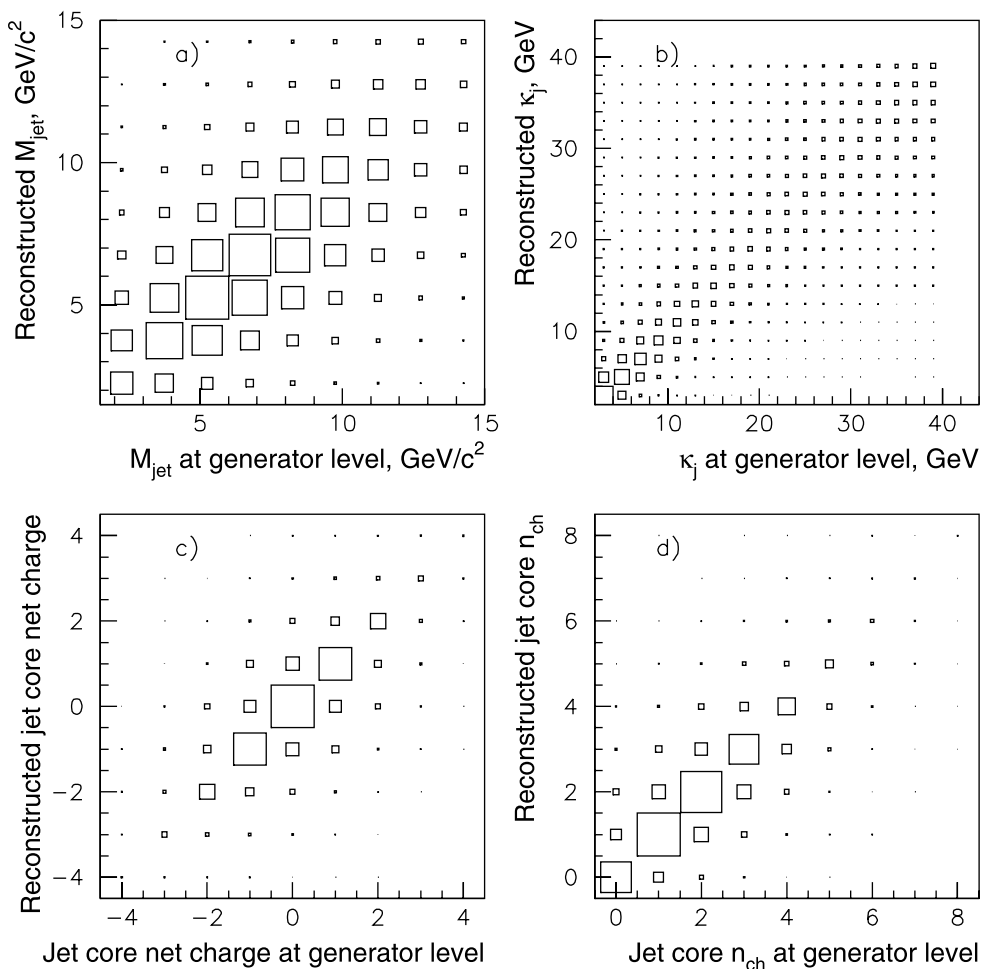
- HPC showers with the energy exceeding 6 GeV were considered as π^0 's;
- converted photons were collected if their energy exceeded 1 GeV;
- HCAL showers were collected if their energy exceeded 2 GeV, and were considered as particles.

The jet neutral particle multiplicity, N_{neu} , has been defined then as the number of its neutral particles, each photon being treated as a half-particle, a π^0 constituent (in the case of half-integer N_{neu} values, they were promoted to the next integers; it was tested that the effect of the π^0 overcounting due to ISR and π^0 photons entering different jets induced by this convention is negligible). For most of the events this effectively means that the neutral particle lower energy cut is 2 GeV. The distributions of the N_{neu} , selected in such a way, are shown in Fig. 1c.

The same criteria were applied to the generated neutral particles. In particular, the photons from neutral pion decays were required to be within the HPC acceptance and to satisfy

Fig. 3 (a) Reconstructed jet mass M_{jet} vs jet mass at the generator level; (b) reconstructed jet variable κ_J vs κ_J at the generator level; (c) reconstructed jet core net charge vs jet core net charge at the generator level; (d) reconstructed jet core n_{ch} vs jet core n_{ch} at the generator level

DELPHI



the energy cuts described above in order for the pion to be counted as a generated neutral particle.

The scatter plot of the reconstructed jet N_{neu} multiplicity versus the jet neutral multiplicity at the generator level is displayed in Fig. 2c. It shows features similar to those of the N_{ch} plot: the prevalence of the main diagonal elements and approximate symmetry of the non-diagonal elements with respect to the diagonal.

In order to keep the N_{neu} systematic bias transparent, columns with the generated neutral multiplicity mean values and their r.m.s. are given in Table 3.

5.5 Jet total particle multiplicity

The term “total particle multiplicity” (or simply “particle multiplicity”), N_{par} , denotes the sum of charged and neutral particles (as defined in the previous sections),

$$N_{\text{par}} = N_{\text{ch}} + N_{\text{neu}},$$

and analogously for the multiplicities at the generator level. The distributions of the N_{par} are shown in Fig. 1d.

The scatter plot of the reconstructed jet N_{par} versus the jet particle multiplicity at the generator level is shown in Fig. 2d. Mean values of the generated particle multiplicities and their r.m.s. are given in Table 4.

5.6 Jet mass and hardness

The jet mass is defined as $M_{\text{jet}}c^2 = \sqrt{E_{\text{jet}}^2 - p_{\text{jet}}^2c^2}$. The distributions of this variable are shown in Fig. 1e. The scatter plot of the reconstructed jet mass M_{jet} versus the mass at the generator level is shown in Fig. 3a.

The jet energy enters also in the variable which characterizes the hardness of the process producing the jet [42, 43], κ_J , which is defined as follows:

$$\kappa_J = E_{\text{jet}} \sin \frac{\alpha}{2},$$

where α is the angle to the closest jet. This variable corresponds to the beam energy in two-jet events without lost

particles. In general, κ_J depends on the topology of the event. Theoretical [42, 43] and experimental [44, 45] studies of hadron production in processes with non-trivial topology have shown that characteristics of the parton cascade depend essentially on this variable. Therefore it was involved in the current analysis, restricting however this particular study to multi-jet (three or more jets) events. A sample of 2 192 644 such events was selected out of the total sample. The distributions of the κ_J variable for these events are shown in Fig. 1f.

The scatter plot of the reconstructed κ_J for jets with momenta $p_{\text{jet}} > 5 \text{ GeV}/c$ versus this variable at the generator level is shown in Fig. 3b.

5.7 Jet core characteristics

5.7.1 Jet core net charge

The jet net charge, Q_{net} , is defined as the algebraic sum of the charges of the jet charged particles. Two kinds of jet net charges were tried, as described in the next two paragraphs, respectively.

The first one was the “raw” jet net charge, with all the jet particles involved. No significant dependence of the soft photon production on this variable was found. Moreover, it has been known for a long time [46] that this variable is ill-defined since it fluctuates significantly depending on whether a positive (negative) soft particle is added to the jet or not. Therefore we leave it out of the presentation of the results.

A more tractable quantity is the jet “core” net charge, which was constructed with those particles only, which had momenta exceeding $2 \text{ GeV}/c$ and were confined within a cone of 100 mrad half-angle to the jet axis. The distributions of this variable are shown in Fig. 1g. The scatter plot of the reconstructed jet core Q_{net} versus this variable at the generator level is shown in Fig. 3c. It shows a good diagonal structure.

In what follows, the absolute values of the core Q_{net} will be used as the corresponding net charge.

5.7.2 Jet core charged multiplicity

The jet core charged multiplicity, core n_{ch} , was defined under the same conditions as the previous variable, i.e. it is the number of jet charged particles having momenta exceeding $2 \text{ GeV}/c$ and confined within a cone of 100 mrad half-angle to the jet axis. The distributions of this variable are shown in Fig. 1h. The scatter plot of the reconstructed jet core n_{ch} versus this variable at the generator level is shown in Fig. 3d. It shows a good diagonal structure.

6 Treatment of systematic errors

6.1 General remarks

In this section the treatment of systematic errors of the photon rates is described. First the systematic uncertainties in the determination of the signal are defined and then those in the bremsstrahlung predictions. The former can be subdivided into the uncertainties originating from the systematic effects biasing the MC distributions with respect to the RD ones (described in Sects. 6.2.1, 6.2.2 below) and the uncertainties common for both data sets (originating from the efficiency corrections, Sect. 6.2.3).

Before going into details of systematic error estimates an important remark on the global values of systematic effects, which might stem from an excess of soft π^0 's and photons from their decays in the real data as compared to the MC, has to be made. These effects were tested in [1] by several methods and were found to be satisfactorily small. In particular, the test invoking almost precise $SU(2)$ symmetry of the strong interactions in order to use charged pions from hadronic decays of Z^0 for evaluation of the possible difference in production rates of neutral pions and, consequently, soft photons in the RD and MC, is described in Sect. 6.2 of [1]. With this test the expectations for the systematic bias of the photon rates in the RD and MC in the signal kinematic range were found to be below 10% of the signal.

Another test, described in Sect. 6.3 of [1], involved the direct comparison of π^0 production in the RD and MC. The upper limit for the systematic bias of the converted soft photon RD to MC ratio obtained from this test was below 20% of the signal at 90% CL. Thus, the two tests agree and suggest that there is no substantial systematic effect due to the modeling and reconstruction of soft photons from π^0 decay.

The methods of the estimation of systematic uncertainties in the determination of the signal in individual bins of the variables under study are described below.

6.2 Systematic uncertainties in the determination of the signal

6.2.1 Event generator systematics

This type of systematic effect arises mainly due to an improper reproduction of the experimental spectra of photons by the MC event generator, being a result of the modeling of the fragmentation process, i.e. parton shower and string hadronization as implemented in [2–4]. Another generator systematic bias which can be induced by an inadequate representation of the full set of unstable hadrons decaying radiatively (other than π^0 's) at the final stage of the hadronization mechanism was carefully studied in [1], and its uncertainty was shown to be small as compared to other components of the systematics; thus it will be neglected in this study.

The systematic errors due to the JETSET fragmentation model and its tuning were estimated in two steps. First, the MC data produced with three different tunings described in [31–33] were analyzed separately in order to extract the systematic error due to the generator tuning. Comparing the photon spectra in the individual bins of variables under study listed in the previous section, this component of the systematic error was determined for every bin of the variables as the r.m.s. of the soft photon rates in the $p_T < 80$ MeV/c region.

Then the MC data produced with ARIADNE were studied. Comparing the photon spectra produced with this generator to those of JETSET, the systematic uncertainties due to the generator model for the rate of soft photons of $p_T < 80$ MeV/c were evaluated for each bin of the variables under study as half the difference between the JETSET and ARIADNE rates.

The typical individual bin systematic error due to the generator was found to be at the level of about (15–25)% of the signal, the main contribution to this error coming from the generator model component.

6.2.2 Detector systematics

This type of systematic effect (called hardware systematics in [1]) is related to biases in the simulation of the detector and experimental conditions in the MC stream, i.e. those which appear when transporting MC photons through the DELPHI setup and reconstructing them (after conversion in the DELPHI setup material) from hits simulated in the TPC. These features have been extensively studied in [1], and a recalibration procedure was elaborated in order to reduce this bias. It used wide angle photons, $\theta_\gamma > 200$ mrad (keeping the $E_\gamma < 1$ GeV), for which the signal of the direct soft photons was assumed to be zero, to re-normalize the material distribution along the photon path in the simulation, and to account for possible differences in reconstruction of converted photons from the TPC hits along e^+e^- tracks in the MC and RD.

The recalibration was applied to each individual bin of the variables described in Sect. 5. Varying the recalibration parameters and the MC data samples, the resulting detector systematic errors for the signal were found to be at the level of about 10% of the signal (on average) after the recalibration.

6.2.3 Systematic errors due to efficiency corrections

The systematic errors due to the method of implementation of the efficiency correction in the photon p_T range below 80 MeV/c were determined individually for every bin of the variables under current study from the MC data and consisted of two components. The first one, induced by an interpolation method, is described in Sect. 3.3. The second

component of this error is a purely instrumental effect originating from the conversion method resolution in energy and the efficiency binning over this variable. It was estimated by comparing the photon p_T distributions taken at the output of the event generator to the analogous distributions of the photons (after they had been transported through the DELPHI detector by DELSIM with a subsequent simulation of their conversions) corrected for efficiency. Both components of the systematic error under discussion were combined in quadrature, resulting in a typical value of the individual bin errors induced by efficiency corrections to be at the level of about 6% of the signal.

These errors were summed quadratically with other components of the signal systematic error described above, thus giving the overall systematic uncertainty in the finding of the signal. However, due to strong bin-to-bin correlations of the systematic errors we will not use them in what follows when fitting signal dependence curves.

6.3 Systematic uncertainty of the bremsstrahlung predictions

The systematic uncertainty for the bremsstrahlung predictions resulting from formula (2) was estimated by comparing the ISR rates obtained with this formula and those delivered by the DYMU3 generator in the photon p_T range (defined to the beam direction) below 80 MeV/c, as the difference between the predictions. This difference was about 4%, and it was taken as the systematic error for the bremsstrahlung predictions.

This value was found to be close to the difference in predictions for the inner hadronic bremsstrahlung rate obtained with formula (2), and those calculated taking into account the higher order radiative corrections, by the use of an exponentiated photon spectrum [23]. When doing these calculations, the β which governs the bremsstrahlung photon spectrum was obtained by integration of formula (3) in [23] applying the p_T cut imposed by the signal definition, $p_T < 0.08$ GeV/c, i.e. within a rather narrow angular range varying as a function of the photon energy according to the aforementioned cut. The β values were found to be 0.0106 and 0.0135 with the minimum jet momentum cut at 5 and 20 GeV/c, respectively, which would lead in both cases to less than 6% difference between formula (2) and exponentiation method predictions.

Another component of the bremsstrahlung prediction error originating from the uncertainties in the charged particle spectra coming from the event generator was determined in [1] to be 5% by varying JETSET tunings and comparison with ARIADNE.

7 Results of the analysis

Throughout this section the dependences of the direct soft photon production on the jet variables will be considered in comparison with those of the inner hadronic bremsstrahlung (often referring to these dependences as to the signal and bremsstrahlung behavior). The overall excess factor of about four over the bremsstrahlung, which can be easily seen in all the tables and plots below, will be taken for granted in the following, even when not explicitly mentioned.

Table 1 The dependence of direct soft photon rates on the jet momentum. The first errors are statistical, the second ones are systematic

$p_{jet},$ GeV/c	$\langle p_{jet} \rangle,$ GeV/c	$\langle p_{jet}^{gen} \rangle,$ GeV/c	Signal, $10^{-3}\gamma/jet$	Bremsstrahlung, $10^{-3}\gamma/jet$
5–10	7.5	8.6	$25 \pm 7 \pm 9$	$5.8 \pm 0.1 \pm 0.4$
10–15	12.4	13.6	$35 \pm 10 \pm 10$	$11.2 \pm 0.1 \pm 0.7$
15–20	17.5	19.6	$68 \pm 12 \pm 17$	$15.6 \pm 0.1 \pm 1.0$
20–25	22.5	25.7	$95 \pm 11 \pm 15$	$18.4 \pm 0.1 \pm 1.2$
25–30	27.6	30.9	$93 \pm 10 \pm 17$	$20.2 \pm 0.1 \pm 1.3$
30–35	32.5	34.8	$83 \pm 9 \pm 16$	$22.2 \pm 0.1 \pm 1.4$
35–40	37.5	37.6	$102 \pm 9 \pm 17$	$24.4 \pm 0.1 \pm 1.6$
40–45	43.4	40.1	$75 \pm 6 \pm 19$	$23.8 \pm 0.1 \pm 1.5$

Table 2 The dependence of direct soft photon rates on the jet charged multiplicity

N_{ch}	$\langle N_{ch} \rangle$	$\langle N_{ch}^{gen} \rangle$	$\langle N_{ch}^{gen} \rangle$ r.m.s.	Signal, $10^{-3}\gamma/jet$	Bremsstrahlung, $10^{-3}\gamma/jet$
0–2	1.68	2.15	1.07	$97 \pm 19 \pm 20$	$12.1 \pm 0.1 \pm 0.8$
3, 4	3.63	4.01	1.15	$65 \pm 9 \pm 12$	$17.0 \pm 0.1 \pm 1.1$
5	5.00	5.30	1.17	$67 \pm 10 \pm 14$	$19.3 \pm 0.1 \pm 1.2$
6	6.00	6.22	1.25	$83 \pm 10 \pm 18$	$20.9 \pm 0.1 \pm 1.3$
7	7.00	7.15	1.33	$90 \pm 11 \pm 18$	$22.7 \pm 0.1 \pm 1.4$
8, 9	8.45	8.45	1.52	$93 \pm 9 \pm 20$	$24.8 \pm 0.1 \pm 1.6$
10, 11	10.41	10.22	1.67	$110 \pm 13 \pm 21$	$27.3 \pm 0.1 \pm 1.7$
12–16	13.19	12.68	2.27	$139 \pm 17 \pm 24$	$29.2 \pm 0.1 \pm 1.9$

Table 3 The dependence of direct soft photon rates on the jet neutral multiplicity

N_{neu}	$\langle N_{neu} \rangle$	$\langle N_{neu}^{gen} \rangle$	$\langle N_{neu}^{gen} \rangle$ r.m.s.	Signal, $10^{-3}\gamma/jet$	Bremsstrahlung, $10^{-3}\gamma/jet$
0	0	0.53	0.74	$41 \pm 11 \pm 16$	$22.3 \pm 0.1 \pm 1.4$
1	1	1.20	0.91	$59 \pm 7 \pm 14$	$22.7 \pm 0.1 \pm 1.4$
2	2	2.15	1.37	$99 \pm 7 \pm 17$	$21.1 \pm 0.1 \pm 1.3$
3	3	2.92	1.50	$115 \pm 10 \pm 24$	$19.1 \pm 0.1 \pm 1.2$
4	4	3.66	1.70	$175 \pm 18 \pm 31$	$17.1 \pm 0.1 \pm 1.1$
5–7	5.18	4.25	1.77	$226 \pm 38 \pm 48$	$13.6 \pm 0.1 \pm 0.9$

7.1 Signal dependence on jet momentum

The distribution of the signal rate against the jet momentum is tabulated in Table 1 and plotted in Fig. 4 (left panel), together with the corresponding predictions for the inner hadronic bremsstrahlung rates. In this figure (as well as in the following ones) the inner vertical bars represent the statistical errors, while the whole vertical bars give the statistical and systematic errors combined in quadrature. The inner hadronic bremsstrahlung predictions are shown in the figure by triangles.³

As can be seen from the figure, the signal rate first increases with the jet momentum, similarly to the predicted bremsstrahlung rate, then it stops increasing, within the errors, at jet momenta about 20 GeV/c. The bremsstrahlung rate also shows a tendency to a saturation with the momentum increase. The curve fitting the bremsstrahlung points is a polynomial of the 2nd order. The same curve scaled by a factor of 3.9 is drawn through the signal points. It describes them well. The ratio of the signal rate to that of the predicted bremsstrahlung is displayed in the right panel of Fig. 4 showing a uniform distribution.

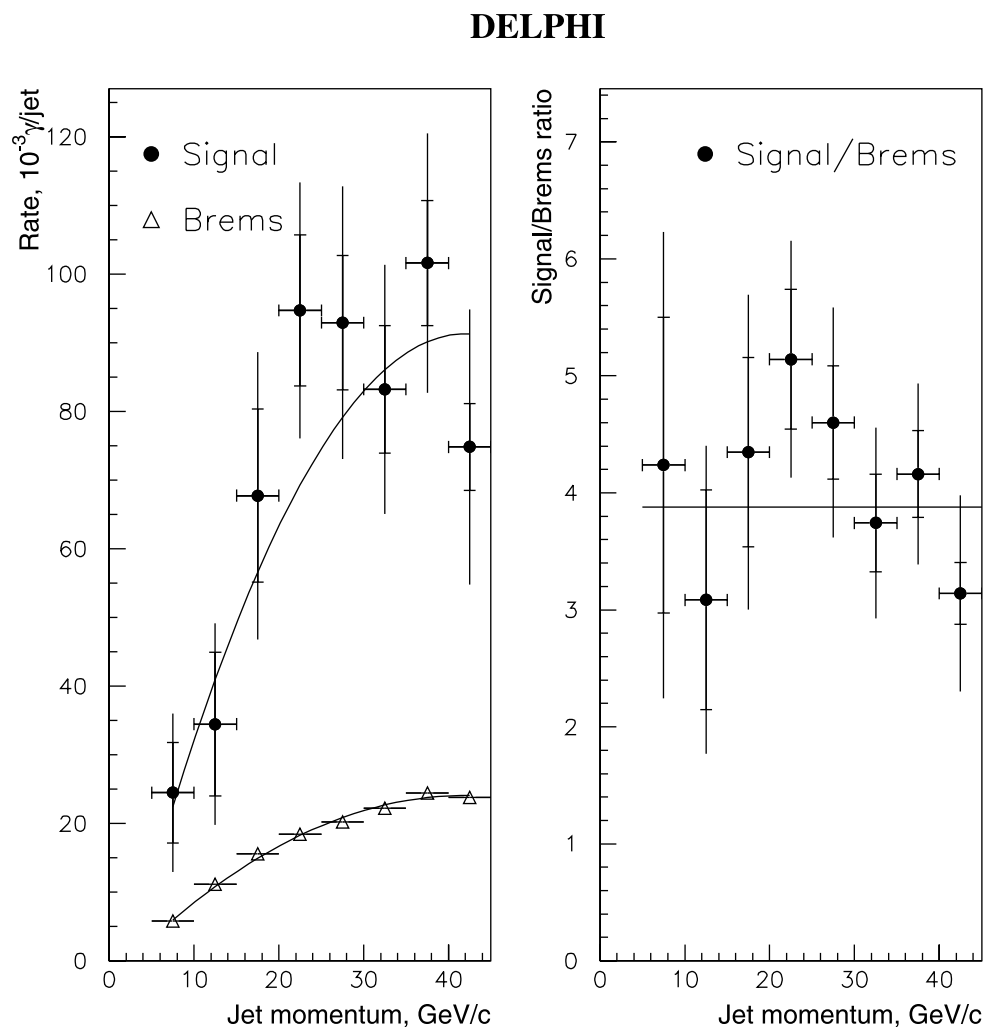
In what follows, only jets with momenta exceeding 20 GeV/c will be taken for the analysis (with one exception for the hardness variable, κ_J). Though general tendencies of the signal behavior with and without this cut are similar, the cut is made in order to separate the momentum and other variable dependences, making use of the weakness of the photon production rate dependence on the jet momenta at $p_{jet} \geq 20$ GeV/c as noticed in the previous paragraph. The integral production rate of direct soft photons obtained with this cut is $(86.3 \pm 4.1 \pm 19.5) \times 10^{-3}\gamma/jet$, while the calculated bremsstrahlung rate is $(21.70 \pm 0.02 \pm 1.39) \times 10^{-3}\gamma/jet$. This can be compared

Table 4 The dependence of direct soft photon rates on the jet total particle multiplicity

N_{par}	$\langle N_{par} \rangle$	$\langle N_{par}^{gen} \rangle$	$\langle N_{par}^{gen} \rangle$ r.m.s.	Signal, $10^{-3}\gamma/jet$	Bremsstrahlung, $10^{-3}\gamma/jet$
1–4	3.50	4.24	1.66	$45 \pm 16 \pm 12$	$18.3 \pm 0.1 \pm 1.2$
5, 6	5.60	6.19	1.72	$51 \pm 9 \pm 11$	$19.2 \pm 0.1 \pm 1.2$
7	7.00	7.46	1.74	$77 \pm 10 \pm 17$	$20.3 \pm 0.1 \pm 1.3$
8	8.00	8.35	1.80	$77 \pm 10 \pm 21$	$21.6 \pm 0.1 \pm 1.4$
9	9.00	9.23	1.85	$81 \pm 11 \pm 20$	$23.2 \pm 0.1 \pm 1.5$
10, 11	10.45	10.50	1.96	$110 \pm 9 \pm 24$	$24.7 \pm 0.1 \pm 1.6$
12, 13	12.41	12.20	2.06	$138 \pm 14 \pm 26$	$27.0 \pm 0.1 \pm 1.7$
14–17	15.16	14.59	2.49	$167 \pm 18 \pm 30$	$28.7 \pm 0.1 \pm 1.8$

³Note, the bremsstrahlung rates given throughout this section are calculated within the bins defined with the detected (not generated) variables.

Fig. 4 Dependence of the direct soft photon production on the jet momentum. *Left panel:* signal and predicted inner bremsstrahlung rates as a function of jet momentum. *Right panel:* ratios of the signal rates to those of the inner bremsstrahlung. *The curves in the left panel* are 2nd order polynomial fits produced to guide the eye; the bremsstrahlung points were fitted first, and then the bremsstrahlung curve was scaled by a factor of 3.9 giving a good approximation to the signal points. The inner vertical bars represent the statistical errors, while the whole vertical bars give the statistical and systematic errors combined in quadrature. *The horizontal line in the right panel* represents the statistical average over the signal-to-bremsstrahlung ratios



to the photon rates obtained without momentum cut, $(69.1 \pm 4.5 \pm 15.7) \times 10^{-3} \gamma/\text{jet}$ for the signal and $(17.10 \pm 0.01 \pm 1.21) \times 10^{-3} \gamma/\text{jet}$ for the inner hadronic bremsstrahlung, which were reported in [1].

7.2 Signal dependence on jet charged multiplicity

The signal dependence on the jet charged multiplicity, as defined in Sect. 5.3, is tabulated in Table 2 and displayed in Fig. 5. As found with the MC $\tau^+\tau^-$ events, the τ channel contaminations (as a fraction of the signal rates in the corresponding bins) in this distribution are:

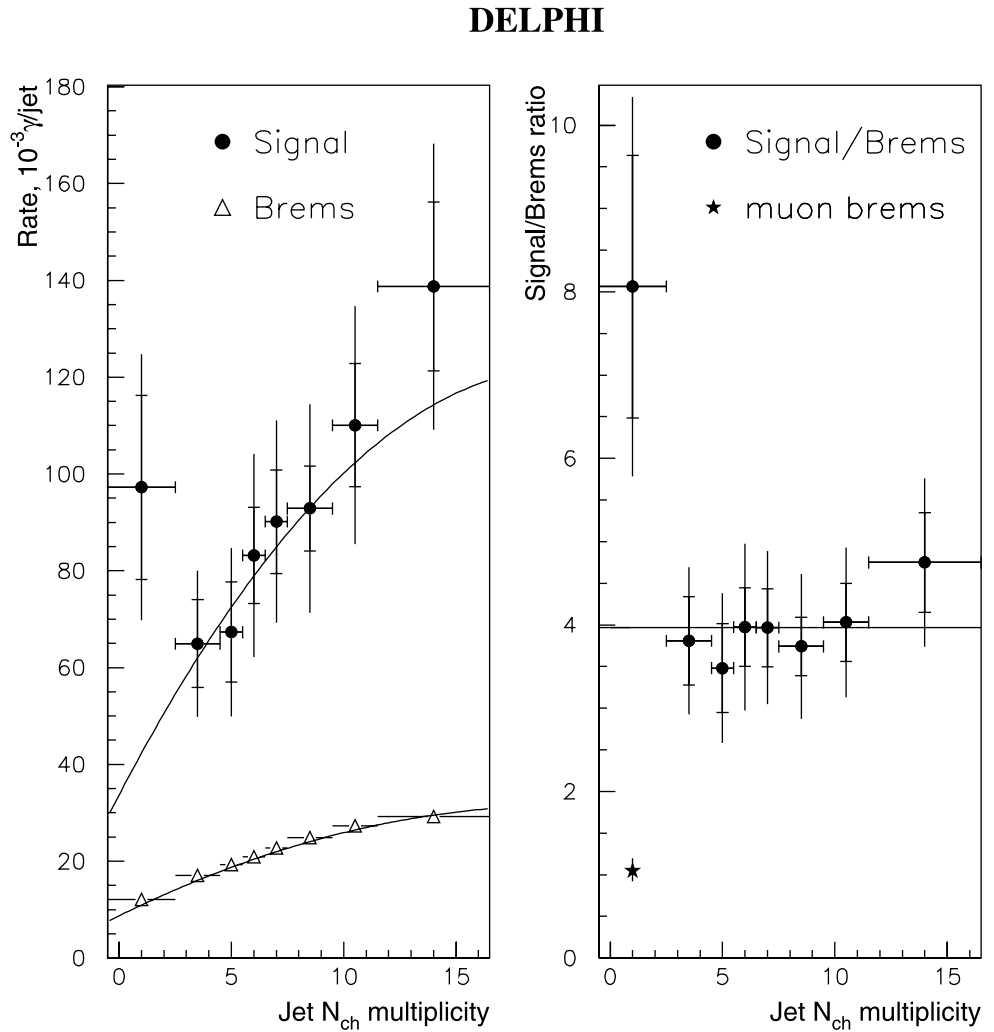
- $(0.3 \pm 0.1)\%$ in the $N_{\text{ch}} = 0 - 2$ bin;
- $(0.1 \pm 0.1)\%$ in the $N_{\text{ch}} = 3, 4$ bin;
- $(0.3 \pm 0.1)\%$ in the $N_{\text{ch}} = 5$ bin;
- $< 0.2\%$ (at 95% CL) in subsequent bins.

As can be seen from Fig. 5, the observed signal rate dependence follows in general, by a scale factor of about 4, that

of the hadronic bremsstrahlung, though there is some excess in the first N_{ch} bin. The curve fitting the bremsstrahlung points in the left panel of Fig. 5 is a 2nd order polynomial. The same curve scaled by a factor of 4 is drawn through the signal points. It describes them satisfactorily, except perhaps the first point. A similar conclusion can be drawn from the plot in the right panel of Fig. 5 in which the ratio of the signal and predicted bremsstrahlung rates is displayed.

Note the muon bremsstrahlung point (an asterisk at the position $N_{\text{ch}} = 1$) in the right panel of Fig. 5. It is placed there using the results of the paper [22] in which a good agreement of the observed inner bremsstrahlung from muons of dimuon events of Z^0 decays with the QED predictions is reported: the ratio of the observed direct soft photon production rate to the predicted level of the muon inner bremsstrahlung was found in [22] to be $1.06 \pm 0.13 \pm 0.06$. This defined the ordinate of the muon point on the plot.

Fig. 5 Dependence of the direct soft photon production on the jet charged multiplicity. *Left panel:* signal and predicted inner bremsstrahlung rates as a function of the jet charged multiplicity. *Right panel:* ratios of the signal rates to those of the inner bremsstrahlung. The curves in the left panel are 2nd order polynomial fits produced to guide the eye; the bremsstrahlung points were fitted first, and then the bremsstrahlung curve was scaled by a factor of 4, which satisfactorily approximates the signal points. The inner vertical bars represent the statistical errors, while the whole vertical bars give the statistical and systematic errors combined in quadrature. The horizontal line in the right panel represents the statistical average over the signal-to-bremsstrahlung ratios. The cut $p_{\text{jet}} \geq 20 \text{ GeV}/c$ is applied



7.3 Signal dependence on jet neutral particle multiplicity

The signal dependence on the jet neutral multiplicity, as defined in Sect. 5.4, is tabulated in Table 3 and shown in Fig. 6.

The contamination from $Z^0 \rightarrow \tau^+\tau^-$ events in the various N_{neu} bins was found to be (as a fraction of the signal rates in the corresponding bins):

- $(1.3 \pm 0.3)\%$ in the $N_{\text{neu}} = 0$ bin;
- $(0.4 \pm 0.1)\%$ in the $N_{\text{neu}} = 1$ bin;
- $(0.2 \pm 0.1)\%$ in the $N_{\text{neu}} = 2$ bin;
- $< 0.2\%$ (at 95% CL) in subsequent bins.

As can be seen from Fig. 6, the signal behavior differs drastically from that of the inner hadronic bremsstrahlung predictions. A possible interpretation of this difference will be given in Sect. 8, when considering various theoretical approaches to the problem of the soft photon excess in reactions of multiple hadron production.

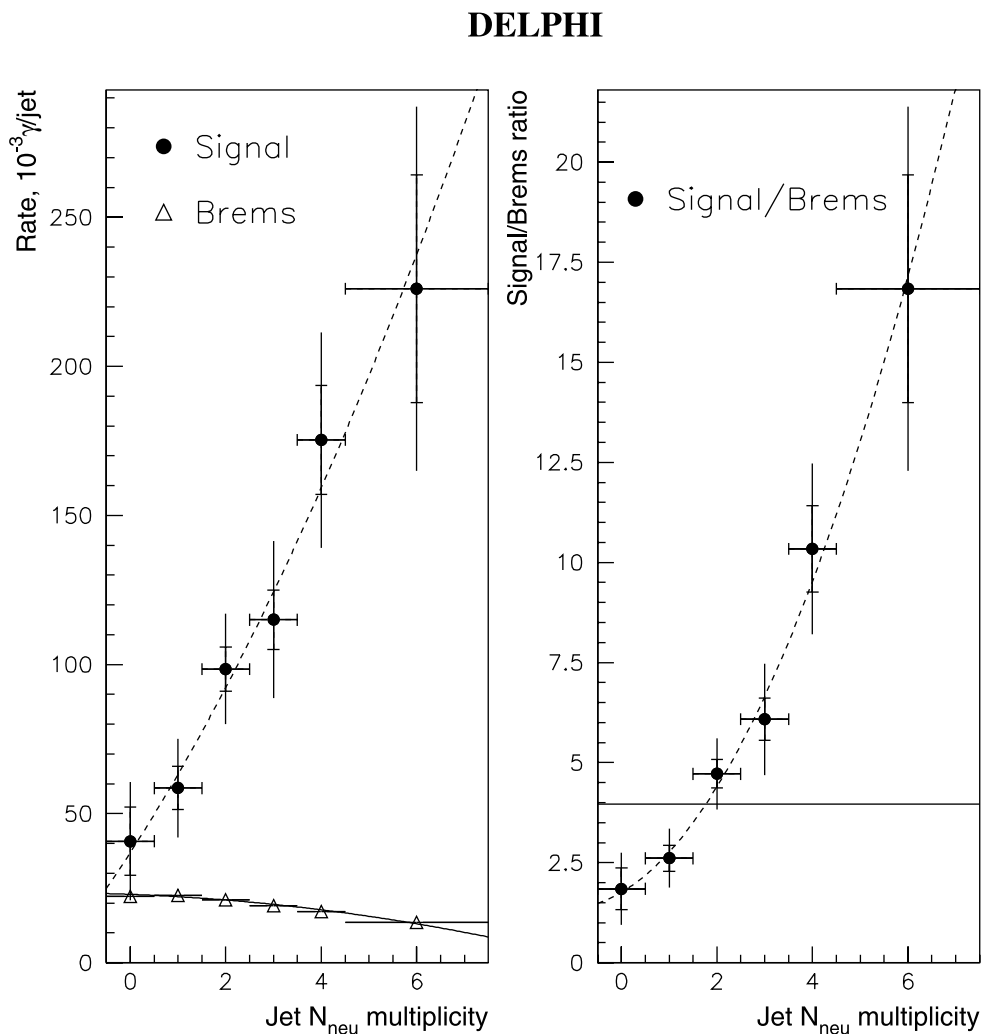
7.4 Signal dependence on the jet total particle multiplicity

The signal dependence on the jet particle multiplicity is given in Table 4 and shown in Fig. 7. The contamination from $Z^0 \rightarrow \tau^+\tau^-$ events in the various particle multiplicity bins was found to be (as a fraction of the signal rates in the corresponding bins):

- $(0.7 \pm 0.2)\%$ in the $N_{\text{par}} = 1 - 4$ bin;
- $(0.3 \pm 0.1)\%$ in the $N_{\text{par}} = 5, 6$ bin;
- $(0.2 \pm 0.1)\%$ in the $N_{\text{par}} = 7$ bin;
- $(0.6 \pm 0.1)\%$ in the $N_{\text{par}} = 8$ bin;
- $(0.9 \pm 0.1)\%$ in the $N_{\text{par}} = 9$ bin;
- $< 0.1\%$ (at 95% CL) in subsequent bins.

As can be seen from Fig. 7, the signal behavior differs from that of the predicted bremsstrahlung, similarly to the previous case. The discussion of this difference is given in Sect. 8. Here we note only that the signal distribution can be fitted satisfactorily by a straight line passing through the origin of the coordinate system, as shown in the left panel of Fig. 7.

Fig. 6 Dependence of the direct soft photon production on the jet neutral multiplicity. *Left panel:* signal and predicted inner bremsstrahlung rates as a function of the jet neutral multiplicity. *Right panel:* ratios of the signal rates to those of the inner bremsstrahlung. All the curves in the figure are independent 2nd order polynomial fits produced to guide the eye. The *inner vertical bars* represent the statistical errors, while the *whole vertical bars* give the statistical and systematic errors combined in quadrature. The *horizontal line* in the *right panel* represents the statistical average over the signal-to-bremsstrahlung ratios. The cut $p_{\text{jet}} \geq 20 \text{ GeV}/c$ is applied



7.5 Signal rates in the 2-dimensional distribution

N_{ch} vs N_{neu}

Due to $SU(2)$ symmetry of the strong interactions and/or selection cuts, the variables N_{ch} and N_{neu} can be correlated. In order to disentangle the signal rate dependences on these variables, the two-dimensional signal distribution as a function of the N_{ch} and N_{neu} was studied. When doing this, the range of the jet polar angles Θ_{jet} to the beam was restricted to the interval of $50^\circ \leq \Theta_{\text{jet}} \leq 130^\circ$. This restriction equalizes, practically, the angular acceptances for the charged and neutral particles, the latter being mainly π^0 's detected by the HPC via their decay photons. This equalization is important when comparing quantitatively the photon rate dependences on the above variables. For the same reason (to equalize detection efficiencies for charged and neutral particles) a lower momentum cut at $2 \text{ GeV}/c$ was introduced when calculating the charged particle multiplicity for this particular analysis.

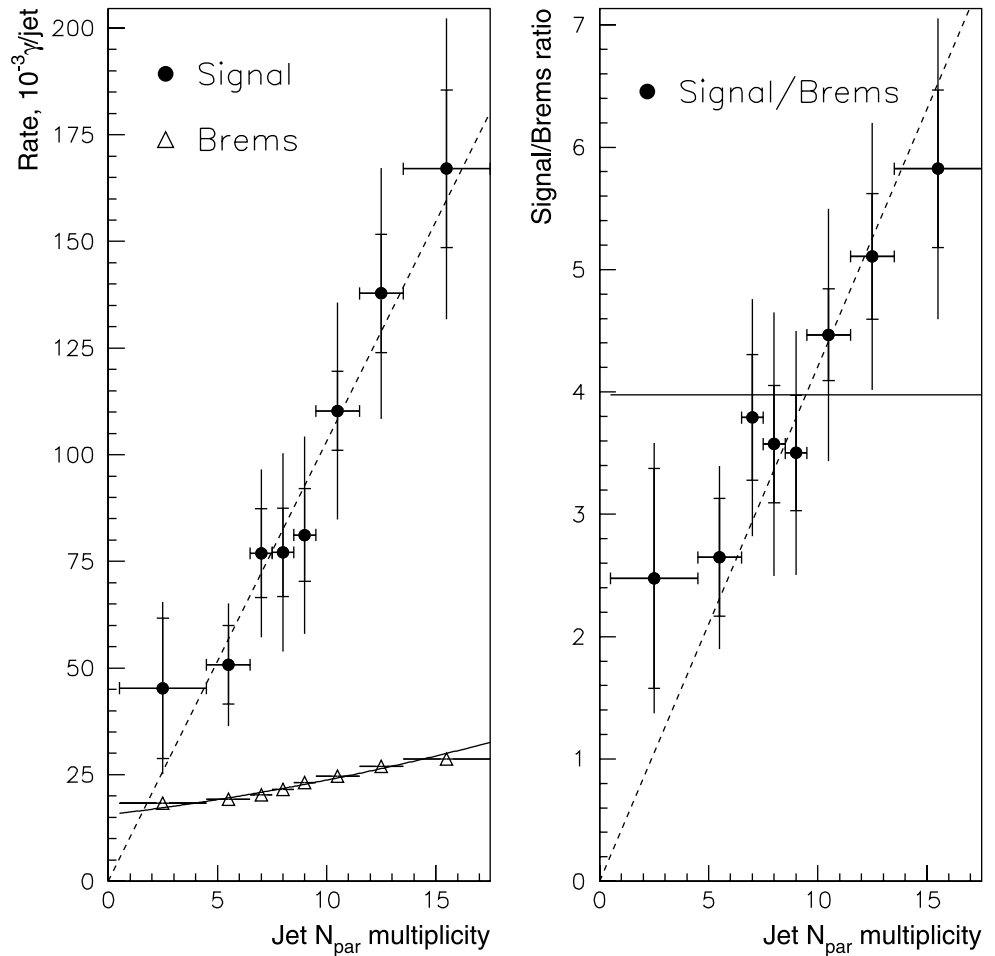
The signal rates obtained with this selection are given as a two-dimensional distribution presented in Table 5.⁴

The distribution was fitted by the simplest possible form $R = a_1 N_{\text{ch}} + a_2 N_{\text{neu}}$ with a reasonable value of the reduced χ^2 close to 1 (the statistical errors only being used in the fit). The values of the fitted rates are given in the last column of Table 5. The linear dependence coefficients a_1 and a_2 obtained with the fit are $(6.9 \pm 1.8 \pm 1.8) \times 10^{-3} \gamma/\text{jet}$ and $(37.7 \pm 3.0 \pm 3.6) \times 10^{-3} \gamma/\text{jet}$, respectively. The first errors of these values are the fit parameter errors based on the statistical errors of the signal rates. The second errors represent the fit parameter changes obtained by adding to the signal rate central values their systematic errors taken randomly accordingly to a Gaussian distribution, and repeating this procedure many times to find at the end the r.m.s. of the

⁴The rates in the 1st and 5th lines of the signal column in Table 5 were corrected for the effect induced by the cut $p_{\text{jet}} \geq 20 \text{ GeV}/c$ after appropriate study of the influence of this cut on the signal rates at small N_{ch} multiplicities, see comment on this influence given in Sect. 7.7.

Fig. 7 Dependence of the direct soft photon production on the jet total multiplicity. *Left panel:* signal and predicted inner bremsstrahlung rates as a function of the jet total multiplicity. *Right panel:* ratios of the signal rates to those of the inner bremsstrahlung. The curve through the bremsstrahlung points in the left panel is a 2nd order polynomial fit produced to guide the eye. The dashed lines in both panels represent the linear fits of the signal points with zero offset to the origin of the coordinate system. The inner vertical bars represent the statistical errors, while the whole vertical bars give the statistical and systematic errors combined in quadrature. The horizontal line in the right panel represents the statistical average over the signal-to-bremsstrahlung ratios. The cut $p_{\text{jet}} \geq 20 \text{ GeV}/c$ is applied

DELPHI



fit parameters; in this way a propagation of the systematic uncertainties of the rates to those of the fit parameters was performed.

A straightforward conclusion which can be drawn from the difference of the two coefficients is that the dependence of the signal rates on the jet neutral multiplicity is a factor of $5.4 \pm 1.4 \pm 1.5$ stronger than the dependence on the charged multiplicity.⁵ A possible interpretation of this difference is suggested in Sect. 8.

7.6 Signal dependence on jet mass and hardness

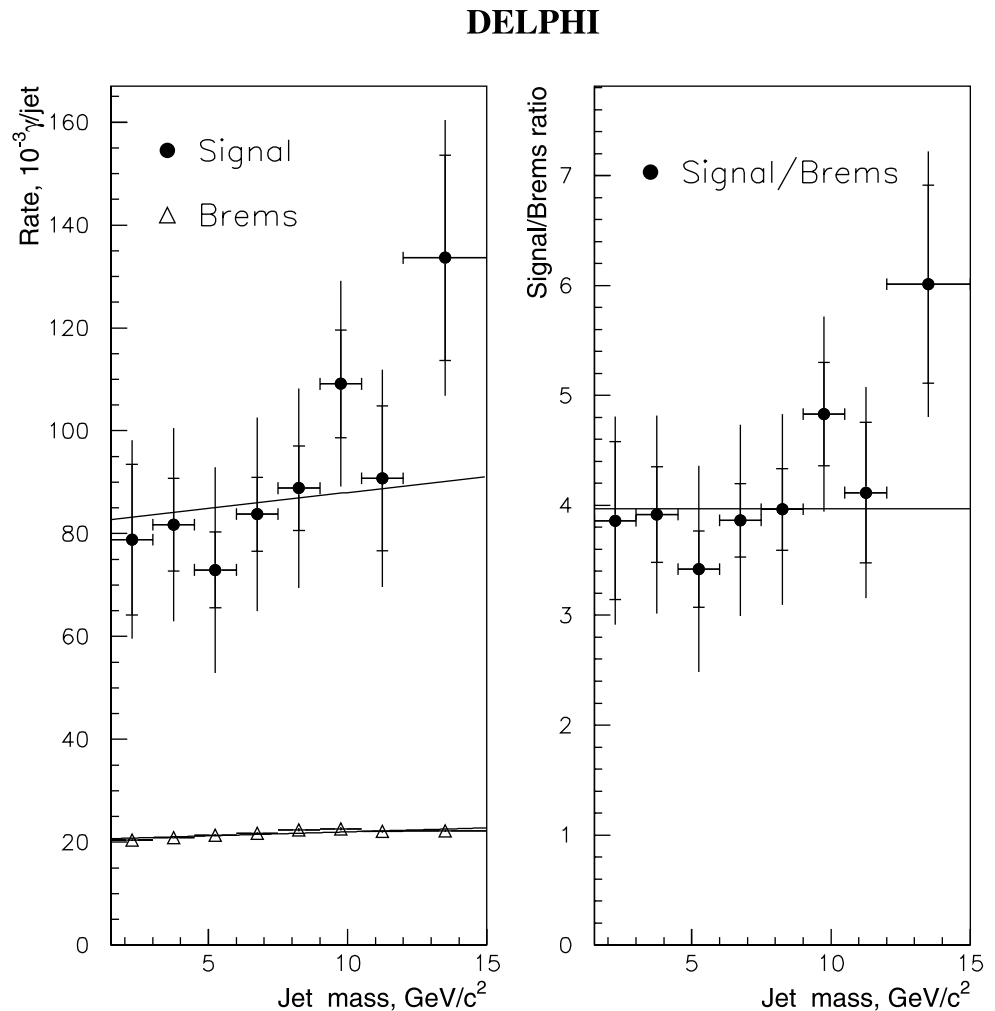
The dependence of the signal rate on the jet mass is given in Table 6 and shown in Fig. 8. As can be seen from the figure, both the signal and the predicted bremsstrahlung rates behave similarly, depending rather weakly on this jet characteristic. Thus the jet mass turns out to be not a very suitable

variable to use for the direct soft photon production rate parameterization. Nevertheless, the observed behavior of the production rates against this variable (the rate flatness) can supply useful information when comparing the various soft photon production models discussed in Sect. 8.

Let us turn now to the hardness variable treated in multi-jet events. As mentioned in Sect. 5.2, the jet momentum cut at $20 \text{ GeV}/c$ was not applied when selecting jets for this particular analysis since the motivation for this cut is not justified in the given case. The integral production rate of direct soft photons obtained with these events is $(63.7 \pm 4.0 \pm 13.9) \times 10^{-3} \gamma/\text{jet}$, while the calculated hadron bremsstrahlung rate is predicted to be $(15.80 \pm 0.01 \pm 1.01) \times 10^{-3} \gamma/\text{jet}$. The observed photon rates (see Table 7 and Fig. 9) show a fast increase with κ_J in the first bins of this variable, followed by a saturation effect above 20 GeV , and they can be fitted satisfactorily by the bremsstrahlung curve scaled by a factor of 4. This means that the observability of a dependence of the direct soft photon production on the hardness, which might differ from the analogous depen-

⁵We have tested that the systematic error of the quoted factor is valid also in the case of strong bin-to-bin correlations of systematic errors of individual photon rates.

Fig. 8 Dependence of the direct soft photon production on the jet mass. *Left panel:* signal and predicted inner bremsstrahlung rates as a function of jet mass. *Right panel:* ratios of the signal rates to those of the inner bremsstrahlung. The curves in the left panel are 1st order polynomial fits produced to guide the eye; the bremsstrahlung points were fitted first, and then the bremsstrahlung curve was scaled by a factor of 4 giving a good approximation to the signal points. The inner vertical bars represent the statistical errors, while the whole vertical bars give the statistical and systematic errors combined in quadrature. The horizontal line in the right panel represents the statistical average over the signal-to-bremsstrahlung ratios. The cut $p_{\text{jet}} \geq 20 \text{ GeV}/c$ is applied



dence of the hadron bremsstrahlung, is below the sensitivity of our approach.

Very similar results were obtained with 2-jet events included in the analysis.

7.7 Signal dependence on the jet core characteristics

The dependences of the signal rate on the jet core net charge and the jet core charged multiplicity are given in Tables 8, 9 and shown in Fig. 10.

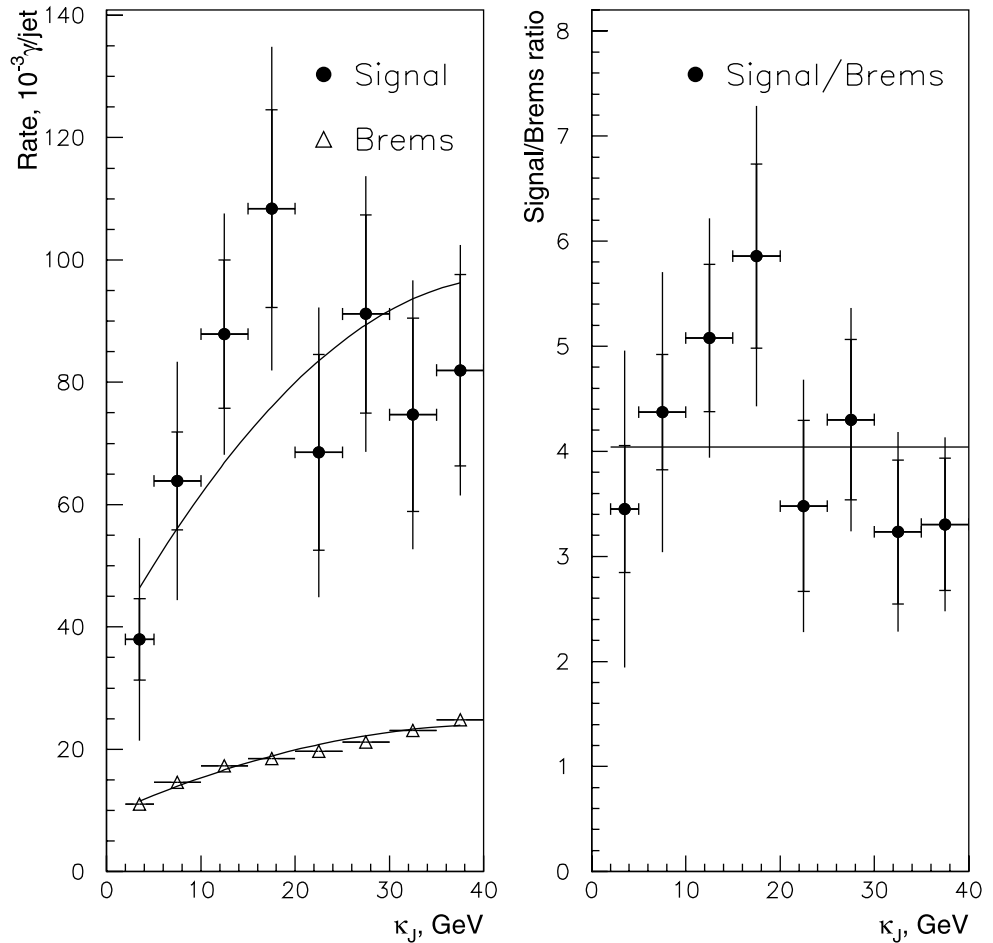
There is a weak dependence (if any) of the signal rate on jet core net charge, while the inner hadronic bremsstrahlung is predicted to grow considerably with it (this prediction follows from the coherent nature of the standard hadronic bremsstrahlung and makes this variable rather interesting from the point of view of distinguishing different models of the anomalous soft photon production considered in Sect. 8).

The linear fit of the bremsstrahlung points results in the slope of the bremsstrahlung dependence on the jet core net charge to be $(4.66 \pm 0.04) \times 10^{-3} \gamma/\text{jet}$ (see solid line in the left upper panel of Fig. 10); an analogous fit of

the signal points (the dashed line in the same panel) gives the value of $(7.6 \pm 5.4) \times 10^{-3} \gamma/\text{jet}$ for the slope. Had the signal the same behavior against this variable as the bremsstrahlung has (scaled simply by a factor of 4), a slope of $18.6 \times 10^{-3} \gamma/\text{jet}$ would be expected. Thus, there is a tendency for the signal dependence on the jet core net charge to deviate from the bremsstrahlung behavior. However, the deviation is not significant (about two standard deviations) and does not allow a conclusion about an essential difference in the dependences of the signal and the bremsstrahlung rates on this variable to be drawn. Nevertheless, a stronger variation (proportional to the net charge squared) which can be assumed for the signal in collective models of the radiation (considered below, Sect. 8.2) can be restricted. An upper limit of 27% of the signal for the quadratic component of the jet core net charge dependence was obtained at 95% CL. This upper limit was calculated by adding a quadratic term to the fit of the dependence, which used a (varied) constant term together with the fixed bremsstrahlung contribution, and increasing the quadratic term yield from zero until

DELPHI

Fig. 9 Dependence of the direct soft photon production on the hardness variable. *Left panel:* signal and predicted inner bremsstrahlung rates as a function of κ_J . *Right panel:* ratios of the signal rates to those of the inner bremsstrahlung. The curves in the *left panel* are 2nd order polynomial fits produced to guide the eye; the bremsstrahlung points were fitted first, and then the bremsstrahlung curve was scaled by a factor of 4 giving a good approximation to the signal points. The *inner vertical bars* represent the statistical errors, while the *whole vertical bars* give the statistical and systematic errors combined in quadrature. The *horizontal line* in the *right panel* represents the statistical average over the signal-to-bremsstrahlung ratios. The cut $p_{\text{jet}} \geq 20 \text{ GeV}/c$ is not applied



the total χ^2 increases by 3.84, the 95% confidence level for the fit with a single degree of freedom.

The dependence of the direct soft photon production rate on the jet core charged multiplicity has apparently a non-trivial behavior, decreasing with the core n_{ch} increase, and getting closer to the bremsstrahlung predictions at higher core n_{ch} . This behavior clearly differs from the signal dependence on the N_{ch} multiplicity presented in Table 5 (such a comparison seems to be most suitable since the cuts on the lower charged particle momenta are identical in both cases). Nevertheless, there is a significant difference between the two selections: in the latter case the selection of charged particles was done with the neutral multiplicity being kept fixed at a certain value, while in the former case it was allowed to vary freely. In particular, the averaged N_{neu} multiplicity decreases from the value of 2.6 (with the r.m.s. of 1.2) in the bin with the core $n_{\text{ch}} = 0$ to the value of 1.7 (with the r.m.s. of 1.1) in the last n_{ch} bin. This anti-correlation, induced mainly by the $p_{\text{jet}} \geq 20 \text{ GeV}/c$ cut (roughly speaking, the smaller is the core n_{ch} , the larger should be N_{neu} in

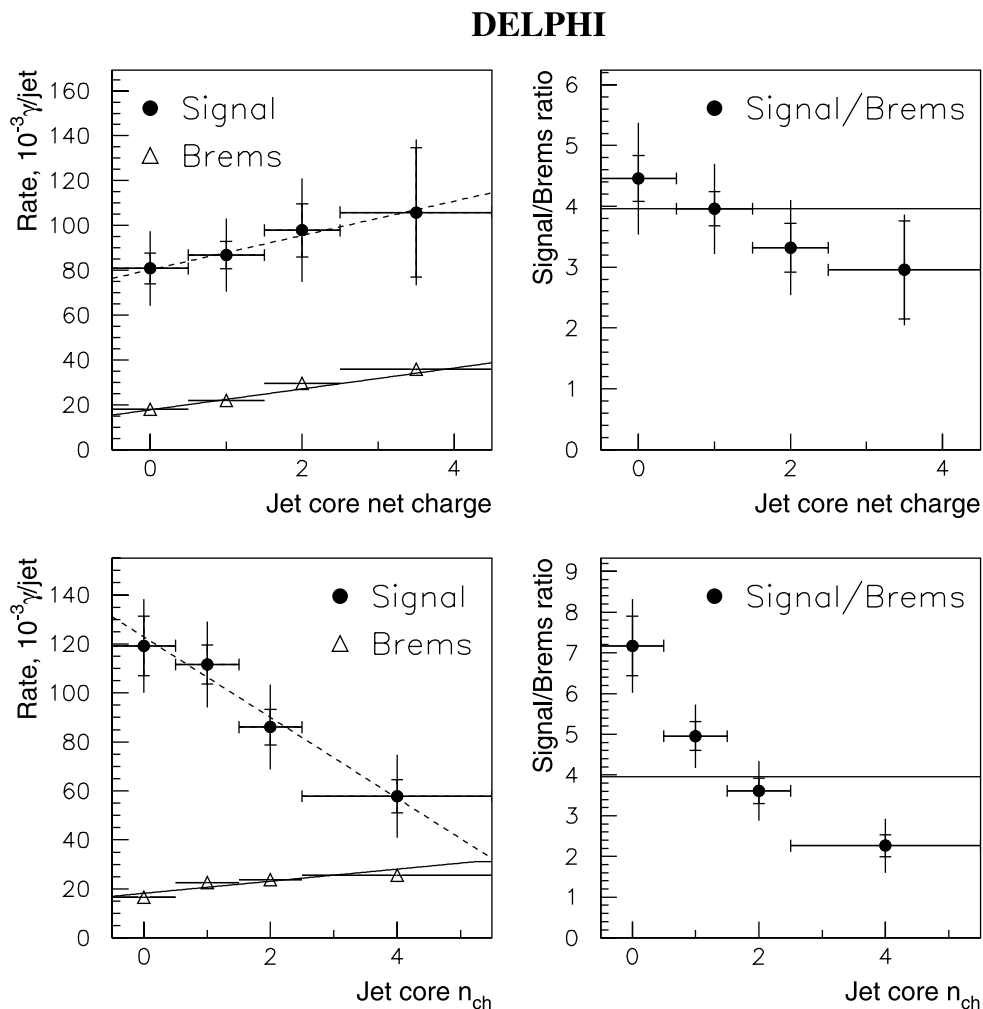
order to satisfy this cut), can be seen in Fig. 1i, where the plot of N_{neu} vs core n_{ch} is given. Since the N_{neu} multiplicity appears to be a variable which governs the soft photon production in hadronic decays of the Z^0 , this anti-correlation may be responsible for the reduction of the photon rates with increasing core n_{ch} . However it is difficult to make a final conclusion on this behavior until a theoretical description of the observed anomalous soft photon production will become available.

8 Discussion of the results

8.1 General remarks

What is the source of the direct soft photon signal in hadronic decays of the Z^0 , which exceeds the level of hadronic bremsstrahlung predictions by a factor of four? Certainly, 25% of the signal can be attributed to the brems-

Fig. 10 Dependence of the direct soft photon production on the jet core characteristics. *Upper panels:* jet core net charge; *bottom panels:* jet core charged multiplicity. *Left panels:* signal and predicted inner bremsstrahlung rates as a function of the jet core characteristics. *Right panels:* ratios of the signal rates to those of the inner bremsstrahlung. The *straight lines in the left panels* are linear fits produced to guide the eye: *solid line* for the bremsstrahlung points and the *dashed line* for the signal. The *inner vertical bars* represent the statistical errors, while the *whole vertical bars* give the statistical and systematic errors combined in quadrature. The *horizontal lines in the right panels* represent the statistical averages over the signal-to-bremsstrahlung ratios. The cut $p_{\text{jet}} \geq 20 \text{ GeV}/c$ is applied



strahlung itself.⁶ Can the rest of the signal be explained by an imperfectness of the standard event generators, used in the analysis, which leads to a huge underestimation of the production of soft photons (and may be soft gluons also) in the fragmentation process, or, at least, by an imperfectness of the photon implementations [26, 47, 48] in the generators? In principle, such a possibility is not excluded. However, it looks quite improbable [49–51], unless new physical effects will be introduced to the generator algorithms. In this section we shall review in brief the general features of theoretical models proposed for the explanation of the soft photon excess in reactions of multiple hadron production, and consider their compatibility with the signal behavior reported in this work.

⁶It is interesting to note that the subtraction of the bremsstrahlung predictions from the signal points measured vs N_{neu} variable (Fig. 6) makes the resulting distribution (not shown) quite linear, with the fit line passing very closely to the origin of the coordinate frame. A similar exercise with the signal distribution vs N_{par} (Fig. 7) improves the χ^2 value of the linear fit mentioned in Sect. 7.4.

The prominent difference of this behavior from the bremsstrahlung one, seen in Figs. 6, 7, demonstrates that the direct soft photon production in hadronic decays of the Z^0 depends not only on the charged hadrons produced, as it would be for the inner hadronic bremsstrahlung, but certainly on the neutral hadrons too. Since the direct coupling of photons to neutral particles (e.g. via magnetic moment) is quite weak, this means that the excess photons under study are coupled either to the individual quarks and/or quark-antiquark pairs constituting a parton shower, or via some collective effect (for example, one of those mentioned in [52]) to a jet as a whole.

The first assumption may enter in an apparent conflict with the expected damping of the soft photon radiation due to coherent effects known as the Landau–Pomeranchuk–Migdal suppression (LPM effect) [53–55], which in the given case would be due to destructive interference between successive photon emitters. However, this remark is valid only when the interference between radiation sources is strong and destructive. In several models aiming at an explanation of the anomalous soft photon effect, the possi-

Table 5 Two-dimensional dependence of direct soft photon rates on the jet multiplicities, N_{ch} versus N_{neu}

N_{ch}	$\langle N_{ch} \rangle$	$\langle N_{ch}^{gen} \rangle$	$\langle N_{ch}^{gen} \rangle$ r.m.s.	Signal, $10^{-3}\gamma/\text{jet}$	Fit, $10^{-3}\gamma/\text{jet}$
Jet $N_{neu} = 0, 1, \langle N_{neu} \rangle = 0.76$					
0, 1	0.91	1.27	0.82	$47 \pm 14 \pm 9$	37
2, 3	2.61	2.87	0.93	$48 \pm 9 \pm 11$	49
4, 5	4.38	4.49	0.99	$63 \pm 10 \pm 12$	61
6–9	6.42	6.26	1.14	$79 \pm 21 \pm 9$	76
Jet $N_{neu} = 2$					
0, 1	0.85	1.27	0.84	$99 \pm 30 \pm 17$	81
2, 3	2.55	2.86	0.93	$116 \pm 29 \pm 31$	93
4, 5	4.36	4.52	0.99	$93 \pm 18 \pm 27$	106
6–9	6.38	6.33	1.08	$121 \pm 39 \pm 19$	120
Jet $N_{neu} = 3$					
0, 1	0.80	1.24	0.87	$111 \pm 26 \pm 19$	119
2, 3	2.51	2.83	0.93	$97 \pm 17 \pm 29$	130
4, 5	4.34	4.52	0.96	$155 \pm 25 \pm 48$	143
6–9	6.31	6.29	1.05	$234 \pm 61 \pm 32$	157
Jet $N_{neu} = 4 - 6, \langle N_{neu} \rangle = 4.40$					
0, 1	0.75	1.20	0.89	$207 \pm 24 \pm 35$	171
2, 3	2.46	2.81	0.95	$170 \pm 21 \pm 47$	183
4, 5	4.29	4.50	0.96	$205 \pm 31 \pm 62$	196
6–9	6.25	6.24	1.06	$256 \pm 91 \pm 94$	209

Table 6 The dependence of direct soft photon rates on the jet mass

$M_{jet},$ GeV/ c^2	$\langle M_{jet} \rangle,$ GeV/ c^2	$\langle M_{jet}^{gen} \rangle,$ GeV/ c^2	Signal, $10^{-3}\gamma/\text{jet}$	Bremsstrahlung, $10^{-3}\gamma/\text{jet}$
1.5–3.0	2.44	3.51	$79 \pm 15 \pm 12$	$20.4 \pm 0.2 \pm 1.3$
3.0–4.5	3.83	4.59	$82 \pm 9 \pm 16$	$20.9 \pm 0.2 \pm 1.3$
4.5–6.0	5.27	5.82	$73 \pm 7 \pm 19$	$21.3 \pm 0.2 \pm 1.4$
6.0–7.5	6.73	7.07	$84 \pm 7 \pm 17$	$21.7 \pm 0.2 \pm 1.4$
7.5–9.0	8.20	8.30	$89 \pm 8 \pm 18$	$22.4 \pm 0.2 \pm 1.4$
9.0–10.5	9.67	9.45	$109 \pm 10 \pm 17$	$22.6 \pm 0.2 \pm 1.4$
10.5–12.0	11.14	10.49	$91 \pm 14 \pm 16$	$22.1 \pm 0.2 \pm 1.4$
12.0–15.0	13.10	11.00	$134 \pm 20 \pm 18$	$22.2 \pm 0.2 \pm 1.4$

bility of interference is discarded or ignored altogether. In the Van Hove and Lichard model of the cold quark-gluon plasma as the source of the soft photons [18, 56, 57], the photon rate is proportional to the (incoherent) sum of cross sections of the photon production in head-on collisions of partons, mainly in the processes of annihilation ($q\bar{q} \rightarrow g\gamma$) and Compton scattering ($qg \rightarrow q\gamma$) (note however a critical remark to this approach with a reference to the LPM effect given in the paper [58]). Also the model [59], based on the Unruh–Davies effect (a purely quantum-mechanical phe-

Table 7 The dependence of direct soft photon rates on the hardness of the process producing the jet, κ_J

$\kappa_J,$ GeV	$\langle \kappa_J \rangle,$ GeV	$\langle \kappa_J^{gen} \rangle,$ GeV	Signal, $10^{-3}\gamma/\text{jet}$	Bremsstrahlung, $10^{-3}\gamma/\text{jet}$
2–5	3.5	3.7	$38 \pm 7 \pm 15$	$11.0 \pm 0.1 \pm 0.7$
5–10	7.1	7.0	$63 \pm 8 \pm 18$	$14.6 \pm 0.1 \pm 0.9$
10–15	12.2	12.2	$87 \pm 12 \pm 15$	$17.3 \pm 0.1 \pm 1.1$
15–20	17.4	17.6	$108 \pm 16 \pm 21$	$18.5 \pm 0.1 \pm 1.2$
20–25	22.5	23.3	$68 \pm 16 \pm 17$	$19.7 \pm 0.1 \pm 1.3$
25–30	27.5	28.2	$90 \pm 16 \pm 16$	$21.2 \pm 0.1 \pm 1.4$
30–35	32.5	32.2	$74 \pm 16 \pm 15$	$23.1 \pm 0.1 \pm 1.5$
35–40	37.5	36.0	$81 \pm 16 \pm 13$	$24.8 \pm 0.1 \pm 1.6$

Table 8 The dependence of direct soft photon rates on the jet core net charge

Q_{net}	$\langle Q_{net} \rangle$	$\langle Q_{net}^{gen} \rangle$	Signal, $10^{-3}\gamma/\text{jet}$	Bremsstrahlung, $10^{-3}\gamma/\text{jet}$
0	0	0.19	$81 \pm 7 \pm 15$	$18.1 \pm 0.1 \pm 1.2$
1	1	0.93	$87 \pm 6 \pm 15$	$22.0 \pm 0.1 \pm 1.4$
2	2	1.70	$98 \pm 12 \pm 20$	$29.5 \pm 0.1 \pm 1.9$
3, 4	3.09	2.56	$106 \pm 29 \pm 15$	$35.8 \pm 0.3 \pm 2.3$

Table 9 The dependence of direct soft photon rates on the jet core charged multiplicity

Core n_{ch}	$\langle \text{Core } n_{ch} \rangle$	$\langle \text{Core } n_{ch}^{gen} \rangle$	Signal, $10^{-3}\gamma/\text{jet}$	Bremsstrahlung, $10^{-3}\gamma/\text{jet}$
0	0	0.13	$119 \pm 12 \pm 15$	$16.6 \pm 0.1 \pm 1.1$
1	1	1.07	$112 \pm 8 \pm 16$	$22.5 \pm 0.1 \pm 1.4$
2	2	2.00	$86 \pm 7 \pm 16$	$23.8 \pm 0.1 \pm 1.5$
3–5	3.40	3.23	$58 \pm 7 \pm 16$	$25.5 \pm 0.1 \pm 1.6$

nomenon which promotes zero-point electromagnetic field fluctuations to the level of real quanta [60] and leads to the thermal radiation from charged particles undergoing acceleration in addition to the bremsstrahlung), assumes an incoherent sum of the radiation intensities from different quarks. Nachtmann’s model of the anomalous soft photons as a synchrotron radiation off quarks [61–63] in the stochastic QCD vacuum [64] also adds the contributions of synchrotron photons from different partons incoherently. This effectively means that the contribution of each quark to the radiation intensity must be proportional to the quark charge squared.

Turning to the models exploiting collective behavior of radiation sources (let us call them collective models for brevity), it is interesting to note that in Barshay’s model of a transient new coherent condition of matter [65–68], proposed for the explanation of the anomalous soft photon production in hadronic beam experiments [9–11], the soft pho-

ton radiation enhancement appears also due to an explicitly non-linear feature of the model, but the radiation itself is coherent and the enhancement occurs due to a *constructive* interference of radiation sources [65].

8.2 Collective models of the radiation

By definition, the collective models assume the presence of some kind of a medium, or an ensemble of particles (in the case relevant to this study, it could be a parton shower containing a big number of constituents). The radiation appearing in the collective models has notably coherent nature since the collective modes of excitation of the medium leading to the radiation are based on the correlations between the radiation sources. Therefore the collective models of the radiation pertain to coherent models. A classical example is the transition radiation induced by a charged particle traversing a boundary between two media with different electric polarizability.⁷ In this case the emerging radiation can be considered as a coherent sum of fields emitted by those parts of the media (polarized by the particle traversing it) which are adjacent to the particle trajectory [70]. In the case of the anomalous soft photon production in reaction (1) some combination of the charged jet constituents (whatever they are, quarks or the final hadrons) would be the basic source of the (coherent) radiation (note, the hadronization time available, namely 100–200 fm/c in lab for jets of 45 GeV, see [71], is big enough to allow the formation of soft photons with transverse momenta of 20–80 MeV/c, which constitute a bulk of the signal, see [1], thus making the coherent approach to the observations reported in this work reasonable).

In this case the production rate of the anomalous photons should depend on the collective jet characteristics, jet net charge and mass. No such dependences were found in the data, as demonstrated by the results described in Sects. 7.6 and 7.7. In particular, the quadratic component of the net charge dependence which can be assumed from Barshay's model [65] was found to contribute less than 27% to the signal (at 95% CL).

Thus the excess photons are unlikely to be produced via some collective effects in jets.

8.3 Incoherent models of the radiation

In these models the production rate of the anomalous soft photons is predicted to be proportional to the sum of the charges squared of quarks constituting the parton shower. Assuming further the proportionality of the number of these

quarks to the total jet particle multiplicity, a linear dependence between the soft photon rate and the mentioned multiplicity can be predicted.

The observed dependence of the soft photon production rate on the total jet particle multiplicity (Fig. 7) agrees well with this hypothesis. A linear fit with zero offset to the coordinate system origin displayed in Fig. 7 describes well the experimental points.

However the assumption of the soft photon rate being simply proportional to the sum of the quark charges squared is unlikely to be reconciled with the prominently different dependences of the rates on the jet charged and neutral particle multiplicities derived in Sect. 7.5. This is a real problem for incoherent models.

8.4 Modification of the incoherent approach

The difference in the dependences of the photon production rates on the jet charged and neutral particle multiplicities can be interpreted more easily in the frame of a $q\bar{q}$ dipole model of the radiation, the dipoles being formed in a parton shower in the fragmentation process. The mean electromagnetic radiation strength of a $q\bar{q}$ dipole is expected to be by an order of magnitude higher for the neutral $q\bar{q}$ pair than that for the charged one.

This expectation follows from the classical (and non-relativistic) consideration of the electric dipole moment of two quarks (the consideration of the dipole moments of $qq\bar{q}$ and $\bar{q}q\bar{q}$ systems is omitted due to their small admixture in a jet). This moment is

$$\vec{d} = \sum_{i=1}^2 q_i \vec{r}_i, \quad (3)$$

where q_i is the electric charge of the quark i , and \vec{r}_i is its radius-vector pointing to the quark from the origin of the comoving coordinate system, which can be fixed at the c.m. position of the quark pair (assuming both quark masses to be equal, the origin can be placed at half the distance between the quarks). The straightforward calculations of dipole moments using this formula show that the neutral dipoles, consisting of opposite quark charges $\pm 1/3$ or $\pm 2/3$ possess a dipole moment which is higher by a factor of 2 or 4, respectively, as compared to the charged dipoles consisting of the quark charges $+1/3$, $+2/3$ or $-1/3$, $-2/3$. For the averaged dipole moments squared the difference (i.e. the difference in the dipole radiation strength) reaches a factor of 10 (note, this estimation of the enhancement factor for neutral $q\bar{q}$ dipoles has to be considered as approximate as being obtained with formula (3) under the aforementioned assumptions).

Decay products of narrow resonances and short-lived unstable particles can decrease this contrast when relating the

⁷An example relevant to the strong interactions (in addition to the already mentioned [65]) can be found in [69] where the model of the coherent hadron production analogous to Cherenkov radiation is suggested.

photon rate to the final particle multiplicities. Nevertheless, the dependence of the photon production rate on the jet total particle multiplicity should remain basically linear, including linear components (corresponding to the radiation from neutral and charged $q\bar{q}$ pairs), though these components should have different weights. Then the following general pattern for the source of anomalous soft photon production emerging from the above considerations can be suggested. It looks as if $q\bar{q}$ pairs consisting of quarks kicked out of the QCD vacuum during the fragmentation process produce extra photons *incoherently* with other $q\bar{q}$ pairs of the jet, while some coherence inside the pairs (considered as radiating dipoles) takes place.

The pairs can consist of $q\bar{q}$ kicked out of the vacuum in space-like separated regions, as in the LUND string model [30] (then some enhancement mechanism is required to explain the strength of the anomalous soft photon signal, as noticed in [51]), or they can appear as closed quark-antiquark loops, as in the model [72–76], which is based on nonperturbative QCD methods applied to the large size systems and contains a strong enhancement mechanism, naturally appearing in this approach. The model was primarily developed for the description of the pion emission by closed $q\bar{q}$ loops of light quarks inside heavy quarkonia, but it can be applied also for an analogous description of the soft photon radiation deep inside jets, which would be a photon source, additional to the bremsstrahlung radiation from the final state hadrons. Preliminary estimations of the soft photon intensity done within this approach look promising [77], and the development of the photon application of the model is in progress.

However currently the details of the radiation mechanism still remain obscure, and a quantitative description of the process by any model is still lacking.

9 Conclusion

An analysis of the direct soft photon production rate as a function of the parent jet characteristics is presented. It contains a study of the dependences of the photon production rates on: (a) jet momenta; (b) jet charged particle multiplicity; (c) jet neutral particle multiplicity; (d) jet total particle multiplicity; (e) jet mass; (f) jet hardness variable; (g) jet core net charge; (h) jet core charged multiplicity.

Apart from the overall excess factor of about four, a good agreement of the direct soft photon behavior as compared to that of the inner hadronic bremsstrahlung predictions is found for the jet momenta, mass and hardness, and a satisfactory agreement for the jet charged multiplicity and the jet core net charge. As to the jet neutral and total multiplicities, as well as for the jet core charged multiplicity, a prominent difference of the observed soft photon signal

from the bremsstrahlung-like behavior is observed. The data especially show that the soft photon production is governed by the multiplicity of neutral hadrons. This, and the linear dependence of the photon rate on the jet total particle multiplicity can be interpreted as a proportionality of the anomalous soft photon radiation to the total number of quark-antiquark pairs produced in the fragmentation process, with the neutral pairs being more effectively radiating than the charged ones. These findings suggest that the anomalous soft photons may shed light on the formation of the primary hadrons and thereby the quark confinement.

Acknowledgements We thank Profs. K.G. Boreskov, F.S. Dzheparov, B. French, A.A. Grigoryan, A.B. Kaidalov, O.V. Kancheli, F.Krauss, A.M. Kunin, W. Ochs, L.B. Okun, R.M. Shahoyan, Yu.A. Simonov, T. Sjöstrand, P. Sonderegger, H.J. Specht, Z. Wąs and C.Y. Wong for fruitful discussions.

We are greatly indebted to our technical collaborators, to the members of the CERN-SL Division for the excellent performance of the LEP collider, and to the funding agencies for their support in building and operating the DELPHI detector.

We acknowledge in particular the support of Austrian Federal Ministry of Education, Science and Culture, GZ 616.364/2-III/2a/98, FNRS-FWO, Flanders Institute to encourage scientific and technological research in the industry (IWT) and Belgian Federal Office for Scientific, Technical and Cultural affairs (OSTC), Belgium, FINEP, CNPq, CAPES, FUJB and FAPERJ, Brazil, Ministry of Education of the Czech Republic, project LC527, Academy of Sciences of the Czech Republic, project AV0Z10100502, Commission of the European Communities (DG XII), Direction des Sciences de la Matière, CEA, France, Bundesministerium für Bildung, Wissenschaft, Forschung und Technologie, Germany, General Secretariat for Research and Technology, Greece, National Science Foundation (NWO) and Foundation for Research on Matter (FOM), The Netherlands, Norwegian Research Council, State Committee for Scientific Research, Poland, SPUB-M/CERN/PO3/DZ296/2000, SPUB-M/CERN/PO3/DZ297/2000, 2P03B 104 19 and 2P03B 69 23(2002-2004), FCT—Fundação para a Ciência e Tecnologia, Portugal, Vedecka grantova agentura MS SR, Slovakia, Nr. 95/5195/134, Ministry of Science and Technology of the Republic of Slovenia, CICYT, Spain, AEN99-0950 and AEN99-0761, The Swedish Research Council, The Science and Technology Facilities Council, UK, Department of Energy, USA, DE-FG02-01ER41155, EEC RTN contract HPRN-CT-00292-2002.

Open Access This article is distributed under the terms of the Creative Commons Attribution Noncommercial License which permits any noncommercial use, distribution, and reproduction in any medium, provided the original author(s) and source are credited.

References

1. J. Abdallah et al. (DELPHI Collaboration), Eur. Phys. J. C **47**, 273 (2006)
2. T. Sjöstrand, Comput. Phys. Commun. **39**, 347 (1986)
3. T. Sjöstrand, M. Bengtsson, Comput. Phys. Commun. **43**, 367 (1987)
4. T. Sjöstrand, *JETSET 7.3 Program and Manual*, CERN-TH/6488-92 (1992)
5. L. Lönnblad, Comput. Phys. Commun. **71**, 15 (1992)
6. G. Marchesini et al., Comput. Phys. Commun. **67**, 465 (1992)

7. F. Low, Phys. Rev. **110**, 974 (1958)
8. V.N. Gribov, Sov. J. Nucl. Phys. **5**, 280 (1967)
9. P.V. Chliapnikov et al., Phys. Lett. B **141**, 276 (1984)
10. F. Botterweck et al., Z. Phys. C **51**, 541 (1991)
11. S. Banerjee et al., Phys. Lett. B **305**, 182 (1993)
12. A. Belogianni et al., Phys. Lett. B **408**, 487 (1997)
13. A. Belogianni et al., Phys. Lett. B **548**, 122 (2002)
14. A. Belogianni et al., Phys. Lett. B **548**, 129 (2002)
15. M.L. Tincknell et al., Phys. Rev. C **54**, 1918 (1996)
16. J. Antos et al., Z. Phys. C **59**, 547 (1993)
17. V. Balek, N. Pišúťová, J. Pišúť, Acta Phys. Pol. B **21**, 149 (1990)
18. P. Lichard, Phys. Rev. D **50**, 6824 (1994)
19. P. Abreu et al. (DELPHI Collaboration), Eur. Phys. J. C **16**, 371 (2000)
20. J. Abdallah et al. (DELPHI Collaboration), Eur. Phys. J. C **45**, 589 (2006)
21. J. Abdallah et al. (DELPHI Collaboration), Eur. Phys. J. C **46**, 295 (2006)
22. J. Abdallah et al. (DELPHI Collaboration), Eur. Phys. J. C **57**, 499 (2008)
23. J. Haisinski, *How to Compute in Practice the Energy Carried away by Soft Photons to all Orders in α* , LAL 87-11 (1987). http://ccdb4fs.kek.jp/cgi-bin/img_index?8704270
24. M. Grabowski, U. Kerres, (SOPHIE/WA83) Internal Note 6.10.87 (Unpublished) (1987)
25. T.J. Brodbeck (for WA83 Collaboration), in *Proceedings of Cragcow Workshop on Multiparticle Production, 1993*, ed. by A. Bialas, K. Fialkowski, K. Zalewski, R.C. Hwa (World Scientific, Singapore, 1993), p. 63
26. T. Sjöstrand, in *Workshop on Photon Radiation from Quarks*, ed. by S. Cartwright, CERN Yellow Report No. 92-04 (1992), p. 103
27. P. Aarnio et al. (DELPHI Collaboration), Nucl. Instrum. Methods A **303**, 233 (1991)
28. P. Abreu et al. (DELPHI Collaboration), Nucl. Instrum. Methods A **378**, 57 (1996)
29. W. Adam et al. (DELPHI Collaboration), Z. Phys. C **69**, 561 (1996)
30. B. Andersson, G. Gustafson, G. Ingelman, T. Sjöstrand, Phys. Rep. **97**, 31 (1983)
31. H. Fürstenau, *Corrected Data Distribution and Monte Carlo Tuning*. DELPHI note 93-17 PHYS-264 (1993)
32. H. Fürstenau, *Tests of QCD and Grand Unified Theories with the DELPHI Detector at LEP*. Ph.D. thesis 04/12/92, University of Karlsruhe (1992); KA-IEKP 92-16 (1992)
33. P. Abreu et al. (DELPHI Collaboration), Z. Phys. C **73**, 11 (1996)
34. S. Jadach, B.F.L. Ward, Z. Wąs, Comput. Phys. Commun. **79**, 503 (1994)
35. J.E. Campagne, R. Zitoun, Z. Phys. C **43**, 469 (1989)
36. J.E. Campagne et al., in: *Z Physics at LEP1*, ed. by G. Altarelli, R. Kleiss, C. Verzegnassi. CERN Yellow Report No. 89-08, vol. 3, 2.2.5, 3.2.5 (1989)
37. P. Abreu et al. (DELPHI Collaboration), Z. Phys. C **68**, 353 (1995)
38. W.T. Eadie et al., *Statistical Methods in Experimental Physics* (North-Holland, Amsterdam, 1982), p. 90
39. T. Sjöstrand, Comput. Phys. Commun. **28**, 229 (1983)
40. S. Moretti, L. Lönnblad, T. Sjöstrand, J. High Energy Phys. **9808**, 0001 (1998). hep-ph/9804296
41. T. Sjöstrand, CERN-TH/7112-93-REV (1995). hep-ph/9508391
42. Yu. Dokshitzer, V.A. Khoze, A. Mueller, S.I. Troyan, in *Basics of Perturbative QCD* (Editions Frontieres, Gif-sur-Yvette, 1991), chap. 9
43. Yu. Dokshitzer, S.I. Troyan, V.A. Khoze, Sov. J. Nucl. Phys. **47**, 881 (1988)
44. P. Abreu et al. (DELPHI Collaboration), Phys. Lett. B **499**, 383 (1999)
45. P. Abreu et al. (DELPHI Collaboration), Eur. Phys. J. C **13**, 573 (2000)
46. R.D. Field, R.P. Feynman, Nucl. Phys. B **136**, 1 (1978)
47. L. Lönnblad, in *Workshop on Photon Radiation from Quarks*, ed. by S. Cartwright, CERN Yellow Report No. 92-04 (1992), p. 109
48. M.H. Seymour, in *Workshop on Photon Radiation from Quarks*, ed. by S. Cartwright, CERN Yellow Report No. 92-04 (1992), p. 113
49. T. Sjöstrand, private communication
50. T. Sjöstrand, in *Workshop on Photon Radiation from Quarks*, ed. by S. Cartwright, CERN Yellow Report No. 92-04 (1992), p. 89
51. B. Andersson, P. Dahlgqvist, G. Gustafson, Nucl. Phys. B **317**, 635 (1989)
52. I.M. Dremin, A.V. Leonidov, Phys.-Uspekhi **38**, 723 (1995)
53. L.D. Landau, I.Ya. Pomeranchuk, Dokl. Akad. Nauk SSSR. **92**, 535 and 735 (1953) (Papers No. 75 and 76 in the English edition of L.D. Landau collected works, Pergamon Press, New York, 1965)
54. A.H. Migdal, Phys. Rev. **103**, 1811 (1956)
55. E.L. Feinberg, I.Ya. Pomeranchuk, Nuovo Cimento Suppl. **III**, 652 (1956)
56. L. Van Hove, Ann. Phys. **192**, 66 (1989)
57. P. Lichard, L. Van Hove, Phys. Lett. B **245**, 605 (1990)
58. E. Quack, P.A. Hennig, Phys. Rev. D **54**, 3125 (1996)
59. S.M. Darbinian, K.A. Ispirian, A.T. Margarian, Sov. J. Nucl. Phys. **54**, 364 (1991)
60. P.W. Milonni, *The Quantum Vacuum* (Academic Press, San Diego, 1993). Sect. 2.10
61. O. Nachtmann, in *Proceedings of 18th Johns Hopkins Workshop on Current Problems in Particle Theory, Florence, 1994* (World Scientific, Singapore, 1994), p. 143. hep-ph/9411345
62. G.W. Botz, P. Haberl, O. Nachtmann, Z. Phys. C **67**, 143 (1995)
63. O. Nachtmann, in *Proceedings of 35th International University School of Nuclear and Particle Physics: Perturbative and Non-perturbative Aspects of Quantum Field Theory, Schlading, 1996*, ed. by H. Latal, W. Schweiger (Springer, Berlin, 1996), p. 49. hep-ph/9609365
64. H.G. Dosch, Yu.A. Simonov, Phys. Lett. B **205**, 339 (1988)
65. S. Barshay, Phys. Lett. B **227**, 279 (1989); [Erratum-ibid. **245**, 687 (1990)]
66. S. Barshay, Part. World **3**, 180 (1994)
67. S. Barshay, P. Heiliger, Z. Phys. C **64**, 675 (1994)
68. S. Barshay, P. Heiliger, Z. Phys. C **66**, 459 (1995)
69. I.M. Dremin, Sov. J. Nucl. Phys. **33**, 726 (1981)
70. J.D. Jackson, *Classical Electrodynamics* (John Wiley and Sons, Inc., New York, 1998), 3rd edn. Sect. 13.7
71. Yu. Dokshitzer, V.A. Khoze, A. Mueller, S.I. Troyan, in *Basics of Perturbative QCD* (Editions Frontieres, Gif-sur-Yvette, 1991), chap. 1
72. Yu.A. Simonov, Phys. A. Nucl. **71**, 1049 (2008). [arXiv:0711.3626](http://arXiv.org/abs/0711.3626)
73. Yu.A. Simonov, JETP Lett. **87**, 121 (2008)
74. Yu.A. Simonov, A.I. Veselov, Phys. Rev. D **79**, 034024 (2009)
75. Yu.A. Simonov, A.I. Veselov, JETP Lett. **88**, 5 (2008)
76. Yu.A. Simonov, A.I. Veselov, Phys. Lett. B **671**, 55 (2009)
77. Yu.A. Simonov, private communication